01 Mar 2015

A Constitutive Model for Entangled Polymers Incorporating Binary Entanglement Pair Dynamics and a Configuration Dependent Friction Coefficient

David W. Mead

Nilanjana Banerjee

Joontaek Park
Missouri University of Science and Technology, parkjoon@mst.edu

Recommended Citation

D. W. Mead et al., "A Constitutive Model for Entangled Polymers Incorporating Binary Entanglement Pair Dynamics and a Configuration Dependent Friction Coefficient," *Journal of Rheology*, vol. 59, no. 2, pp. 335-363, American Institute of Physics (AIP), Mar 2015.
The definitive version is available at https://doi.org/10.1122/1.4905921

A constitutive model for entangled polymers incorporating binary entanglement pair dynamics and a configuration dependent friction coefficient

Article *in* Journal of Rheology · March 2015
DOI: 10.1122/1.4905921

CITATIONS
5

READS
138

3 authors, including:

Joontaek Park
Missouri University of Science and Technology
33 PUBLICATIONS **100** CITATIONS

SEE PROFILE

A constitutive model for entangled polymers incorporating binary entanglement pair dynamics and a configuration dependent friction coefficient

David W. Mead

1 Alder Way, Bedford, New Hampshire 03110

Nilanjana Banerjee and Joontaek Park[a)]

Chemical and Biochemical Engineering Department, Missouri University of Science and Technology, Rolla, Missouri 65409

(Received 7 September 2014; final revision received 31 December 2014; published 16 January 2015)

Synopsis

Following recent work [e.g., J. Park *et al*., J. Rheol. **56**, 1057–1082 (2012); T. Yaoita *et al*., Macromolecules **45**, 2773–2782 (2012); and G. Ianniruberto *et al*., Macromolecules **45**, 8058–8066 (2012)], we introduce the idea of a configuration dependent friction coefficient (CDFC) based on the relative orientation of Kuhn bonds of the test and surrounding matrix chains. We incorporate CDFC into the "toy" model of Mead *et al*. [Macromolecules **31**, 7895–7914 (1998)] in a manner akin to Yaoita *et al*. [Nihon Reoroji Gakkaishi **42**, 207–213 (2014)]. Additionally, we incorporate entanglement dynamics (ED) of discrete entanglement pairs into the new Mead–Banerjee–Park (MBP) model in a way similar to Ianniruberto and Marrucci [J. Rheol. **58**, 89–102 (2014)]. The MBP model predicts a deformation dependent entanglement microstructure which is physically reflected in a reduced modulus that heals slowly following cessation of deformation. Incorporating ED into the model allows "shear modification" to be qualitatively captured. The MBP model is tested against experimental data in steady and transient extensional and shear flows. The MBP model captures the monotonic thinning of the extensional flow curve of entangled monodisperse polystyrene (PS) melts [A. Bach *et al*., Macromolecules **36**, 5174–5179 (2003)] while simultaneously predicting the extension hardening found in PS semidilute solutions where CDFC is diluted out [P. K. Bhattacharjee *et al*., Macromolecules **35**, 10131–10148 (2002)]. The simulation results also show that the rheological properties in nonlinear extensional flows of PS melts are sensitive to CDFC but not to convective constraint release (CCR) while those for shear flows are influenced more by CCR. The monodisperse MBP toy model is generalized to arbitrary polydispersity. © *2015 The Society of Rheology*. [http://dx.doi.org/10.1122/1.4905921]

I. INTRODUCTION

The idea of a configuration dependent friction coefficient (CDFC), which is based on the relative orientation of a test chain *segment* to the surrounding matrix chain segments, was previously introduced by Park *et al*. (2012). Although related through a Kuhn–Grün analysis

[a)]Author to whom correspondence should be addressed; electronic mail: parkjoon@mst.edu

[e.g., Larson (1988)], a better, more fundamentally based proposition is to base CDFC on the relative orientation of the Kuhn bonds of the test and matrix chains, respectively [Ianniruberto *et al.* (2011, 2012) and Yaoita *et al.* (2012, 2014)]. Since CDFC impacts both the stretch (Rouse) and terminal relaxation times equally, CDFC can in principle capture the monotonic thinning of the extensional flow curve of entangled monodisperse polystyrene (PS) melts [Bach *et al.* (2003)] while simultaneously predicting the extension hardening found in entangled monodisperse PS solutions where the effects of CDFC are negligible due to dilution [Bhattacharjee *et al.* (2002); Desai and Larson (2014)].

In addition to altering the form of CDFC employed, we shall also address other fundamental issues in molecular modelling the rheology of polymer melts. In particular, the mono and polydisperse MLD models [Mead *et al.* (1998)] assume a *constant* entanglement density in all flow situations. This fundamental assumption is almost certainly *wrong*. Theoretically, the assumption of a constant entanglement density is reflected in the fact that the equilibrium plateau modulus is used to scale the stress in all tube models, i.e., the GLaMM model [Graham *et al.* (2003)], all Doi–Edwards type models such as the MLD model [Mead *et al.* (1998); Mead (2007)], and the pom-pom model [McLeish and Larson (1998)]. It is difficult to understand how the equilibrium plateau modulus can be used to scale stress levels in the highly nonlinear flow regime since reductions in the entanglement density have been demonstrated in nonequilibrium molecular dynamics simulations of shear flow [Baig *et al.* (2010)] and detailed molecular models [Andreev *et al.* (2013)]. Additionally, interrupted transient step shear rate rheological data on linear and long-chain branched (LCB) polyethylene melts by Dealy and Tsang (1981) (and references therein) strongly support the idea of a dynamic entanglement network. These theoretical and experimental results suggest that a fundamental reappraisal is appropriate for the formulation of molecular constitutive models that span the full range of flows from linear viscoelasticity to the nonlinear fast flow regime of linear and LCB polymer melts.

In this paper, we develop a new molecular model based on the dynamics of discrete entanglement pairs (entanglement dynamics: ED) as opposed to traditional mean field tube descriptions [Desai and Larson (2014)]. Adopting this description is supported by recent atomistic simulations which reveal the nature of an entanglement to be that of a topological coupling of a discrete pair of chains [Everaers *et al.* (2004); Tzoumanekas and Theodorou (2006); Baig *et al.* (2010)]. Both the modulus and the terminal disengagement time are functions of the entanglement density and changes to the entanglement density will directly impact these quantities. This paper seeks to incorporate a quantitative description of entanglement pair dynamics and a Kuhn bond based CDFC into the mono and polydisperse MLD toy models. This will yield a general molecular constitutive model at the theoretically and computationally simple toy level that can handle arbitrary polydispersity in arbitrarily fast flows.

This paper is organized as follows: In Sec. II, we introduce a toy dynamical equation for entanglement pairs in monodisperse systems. In Sec. II A, we define the specific form of CDFC we shall use for monodisperse systems. Section III reviews aspects of the Desai–Larson modified DEMG model {Doi–Edwards–Marrucci–Grizzuti [Pearson *et al.* (1991); Mead and Leal (1995); Mead *et al.* (1995)]} which will serve as a base case for the current work. Section IV introduces two new effects we anticipate will impact the dynamics of highly oriented systems. Section V summarizes the new monodisperse toy molecular model incorporating all the features presented in Secs. II–IV. Steady and transient uniaxial extension is simulated and compared with experimental data in Sec. VI. Steady and transient simulations are also performed for shear flow in Sec. VI A. The results of our new molecular model are discussed and summarized in Sec. VII.

II. MODELLING THE ENTANGLEMENT PAIR DYNAMICS FOR MONODISPERSE SYSTEMS

We begin by constructing a toy dynamical equation for the number of entanglements on a chain in a monodisperse melt. This is inspired by analogy to the slip-link EDs in the stochastic simulator [Park *et al*. (2012)] and the discrete slip-link model of Andreev *et al*. (2013) and is similar in spirit to transient network models [Mewis and Denn (1983)]. Ianniruberto and Marrucci (2014) have independently pursued conceptually similar arguments to those presented below to construct a dynamical equation for the entanglement density

$$\dot{N}(t) = \underbrace{\frac{N_e - N(t)}{\tau_d^1(t)}}_{\text{test chain tip diffusion}} \underbrace{-\beta\left[(\boldsymbol{\kappa} : \mathbf{S}_{tube}) - \frac{\dot{\Lambda}(t)}{\Lambda} + \frac{\dot{\alpha}(t)}{\alpha}\right]N(t)}_{\substack{\text{convective destruction} \\ \text{of entanglements}}} + \underbrace{\frac{N_e - N(t)}{\tau_d^1(t)}}_{\text{matrix tip diffusion}} . \quad (1)$$

Here, $N(t)$, represents the number of entanglement pairs per polymer chain at the current time, t while $N_e \equiv (M/M_e)$ represents the average equilibrium number of entanglement pairs per chain of molecular weight M with entanglement molecular weight M_e. The nonequilibrium tube disengagement time is $\tau_d^1(t)$. In the second term on the right-hand side (RHS), β is a parameter that reflects the "efficiency" of the convective constraint release mechanism (CCR). The velocity gradient is given by $\boldsymbol{\kappa}$ and the orientation tensor is defined by $\mathbf{S}_{tube} \equiv \langle \hat{R}\,\hat{R}\,\rangle$, where $\hat{R}$ is the unit end-to-end vector of a tube segment. The relative stretch of the "partially disentangled" chain variable is defined by $\Lambda(t) \equiv [L(t)/L_{eq}(t)]$, where $L(t)$ is the current tube contour length and $L_{eq}(t)$ is the equilibrium length. Note here that $\Lambda(t)$ is different from the relative stretch of a "fully entangled" chain relative to the initial equilibrium length, which is defined as $\lambda(t) \equiv [L(t)/L_{eq}]$. Additionally, the ratio between the maximum stretch ratios of both relative stretches is defined as $\alpha(t) \equiv [\Lambda_{\max}(t)/\lambda_{\max}]$.

What Eq. (1) represents is the idea that entanglements are destroyed by CCR in proportion to the current entanglement density, $N(t)$, times the fractional rate at which they are destroyed via convection. Entanglements are created by tip diffusion/fluctuations of the test chain and the matrix chains at a rate in proportion to the difference between the entanglement density and its equilibrium value, a driving force, divided by the time scale for the process, $\tau_d^1(t)$.

We now derive the entanglement destruction term in Eq. (1), more specifically the expression for the fractional rate of convective destruction of entanglements: $\{(\boldsymbol{\kappa} : \mathbf{S}_{tube}) - [\dot{\Lambda}(t)/\Lambda] + [\dot{\alpha}(t)/\alpha]\}$. Since $L_{eq}(t)$ is a function of the entanglement density $N(t)$, i.e., $L_{eq}(t) \sim \sqrt{N(t)}$ (see Eq. (A3) of Appendix A), differentiating $\Lambda(t) \equiv [L(t)/L_{eq}(t)]$ with respect to time and simplifying yields

$$\frac{\dot{L}(t)}{L(t)} = \underbrace{\frac{\dot{L}_{eq}(t)}{L_{eq}(t)}}_{\substack{\text{Internal rearrangements} \\ \text{of the chain contour} \\ \text{due to CR driven disentanglement}}} + \underbrace{\frac{\dot{\Lambda}(t)}{\Lambda(t)}}_{\substack{\text{Fractional rate} \\ \text{of tube stretch} \\ \text{via all mechanisms}}} = \frac{1}{2}\frac{\dot{N}(t)}{N(t)} + \frac{\dot{\Lambda}(t)}{\Lambda(t)}. \quad (2)$$

The fractional rate of change of the tube contour length $[\dot{L}(t)/L(t)]$ has two separate contributions. The first term on the RHS of Eq. (2) is new and represents the fractional tube shortening/lengthening rate due to constraint release (CR) driven disentanglement. The second term on the RHS represents the fractional rate of tube stretching due to affine

stretch, chain retraction of the chain tips into interior parts of the chain, and CCR driven tube shortening. All of the effects contained within the second term on the RHS have been presented in Mead *et al.* (1998) and discussed in detail there. Only the disentanglement term, $[\dot{L}_{eq}(t)/L_{eq}(t)] = (1/2)[\dot{N}(t)/N(t)]$, is new. However, even this term is discussed in Sec. II A 2 of Mead *et al.* (1998). Note that in the original MLD model the entanglement density was assumed to be *constant*, $\dot{N} = 0$.

From Eq. (16) or Eq. (29), we determine that $[\dot{\alpha}(t)/\alpha] = -(1/2)[\dot{N}(t)/N(t)]$ so we finally have an expression for $[\dot{L}(t)/L(t)]$ in terms of Mead–Banerjee–Park (MBP) model terms

$$\frac{\dot{L}(t)}{L(t)} = \frac{1}{2}\frac{\dot{N}(t)}{N(t)} + \frac{\dot{\Lambda}(t)}{\Lambda(t)} = -\frac{\dot{\alpha}(t)}{\alpha} + \frac{\dot{\Lambda}(t)}{\Lambda(t)}. \tag{3}$$

Thus, calculating $[\dot{L}(t)/L(t)]$ is straightforward in the MBP model. Equation (3) for $[\dot{L}(t)/L(t)]$ can be used directly in Eq. (9) defining k of the MLD paper [Mead *et al.* (1998), p. 7901]

$$k \equiv (\boldsymbol{\kappa} : \mathbf{S}) - \frac{\dot{L}(t)}{L(t)} = \left[(\boldsymbol{\kappa} : \mathbf{S}) - \frac{\dot{\Lambda}(t)}{\Lambda} + \frac{\dot{\alpha}(t)}{\alpha}\right] \approx \left[(\boldsymbol{\kappa} : \mathbf{S}) - \frac{\dot{\Lambda}(t)}{\Lambda}\right]. \tag{4}$$

Generally, $|(\boldsymbol{\kappa} : \mathbf{S}) - (\dot{\Lambda}(t)/\Lambda)| \gg |(\dot{\alpha}(t)/\alpha)|$ which when valid reduces Eq. (4) to the same CCR expression in the original MLD model. We use the expression for k (4) in the convective destruction of entanglements term in Eq. (1) as well as in the stretch equation and orientational relaxation equation, both of which include CCR, in the MBP model.

Note that we have ignored factors of Λ^2 in the denominator of the reptative diffusion entanglement creation/destruction terms in Eq. (1). We ignore this factor in light of the fact that we are not considering contour length fluctuations explicitly. Contour length fluctuations have no such factor scaling the diffusive creation/destruction of entanglements. Tip contour length fluctuations are presumably responsible for most of the diffusive entanglement creation/destruction processes. However, for the newly created tip entanglement to diffuse into the interior of the chain, it takes the reptation time. Hence using the bare reptation time as a characteristic time scale for entanglement creation is a compromise in this simple toy version of the model. A tube coordinate is needed to have a proper description of the entanglement creation/destruction processes. The model of Andreev *et al.* (2013) provides just such a description in a detailed way. Experimentally, studies of the re-entanglement kinetics/dynamics from virgin (unentangled), nascent polymer melts provide a viable means to quantitatively determine the appropriate time scale for the re-entanglement processes described in Eq. (1) [Yamazaki *et al.* (2006); Rastogi *et al.* (2003); Wang *et al.* (2009)].

The factor β scaling the convective destruction of entanglements term represents a CCR efficiency factor related to the number of CR events required to generate a single disentanglement [Ianniruberto and Marrucci (1996)]. This interpretation suggests that $0 < \beta < 1$. The factor β was originally introduced by Ianniruberto and Marrucci (1996, 2001) to ensure a stable monotonic steady shear stress vs shear rate curve and β retains this interpretation in the current work.

The nonequilibrium tube disengagement time $\tau_d^1(t)$ is a function of the entanglement density, $N(t)$. Physically, this arises because the absolute distance for the chain to diffuse shortens as the number of entanglements decreases. In Appendix A, we derive the result

$$\tau_d^1(t) = \left(\frac{N(t)}{N_e}\right)\tau_{d,0}(t). \tag{5}$$

Here, $\tau_d^1(t)$ is the terminal tube disengagement time for arbitrary $N(t)$ relative to the nonequilibrium tube disengagement time, $\tau_{d,0}(t)$, which will be lowered in fast flows by CDFC and hence is also a function of time (Sec. II A).

Using Eq. (5) in Eq. (1) the expression for the EDs can now be simplified and rewritten as

$$\dot{N}(t) = \underbrace{\frac{2N_e}{\tau_{d,0}(t)}\left[\frac{N_e}{N(t)} - 1\right]}_{\substack{\text{entanglement creation} \\ \text{via tip diffusion}}} \quad \underbrace{-\beta\left[(\boldsymbol{\kappa} : \mathbf{S}_{tube}) - \frac{\dot{\Lambda}(t)}{\Lambda} + \frac{\dot{\alpha}(t)}{\alpha}\right]N(t)}_{\text{CCR induced entanglement destruction}}. \tag{6}$$

Note that the MLD toy model for ED does not explicitly contain tip fluctuations which are undoubtedly very important in the re-entanglement process [Mead (2011b); Andreev *et al.* (2013)]. A more detailed model at the tube coordinate level is needed to properly capture the effects of tip fluctuations versus reptational effects.

The modulus scales the stress in molecular models and is a function of the entanglement density. It can be written as [Dealy and Wissbrun (1989)]

$$G_N(t) \equiv \frac{\rho RT}{M_e(t)} = \frac{\rho RT}{\left(\frac{M}{N(t)}\right)} = \frac{N(t)}{N_e}G_N^0. \tag{7}$$

Here, G_N^0 is the equilibrium plateau modulus. ρ, R, and T are density, gas constant, and absolute temperature, respectively. If the entanglement density is significantly lower than equilibrium, the modulus will be directly impacted (lowered) for an extended period of time following deformation. This could explain the phenomena of shear modification which is still unexplained theoretically [Rokudai (1979); Yamaguchi and Wagner (2006); Leblans and Bastiaansen (1989)]. Shear modification is a deformation-induced reversible reduction in the dynamic moduli for high molecular weight polydisperse linear and LCB entangled polymers [Dealy and Wissbrun (1989)]. Shear modification is one of the last great unsolved theoretical problems in nonlinear molecular rheology.

One of the conundrums with the above EDs model is that in very fast extension virtually all the entanglements are convected away leaving a modulus that approaches zero. Not surprisingly the discrete slip-link model by Andreev *et al.* (2013) has similar issues. When all entanglements are stripped from the chain, the Peterlin modulus will be applicable [Desai and Larson (2014)]. The Peterlin modulus is that of an unentangled ensemble of stretched chains in a flow field.

A. Formulation of the expression for Kuhn bond based CDFC on the stretch and terminal orientational relaxation times

Here, we briefly outline how to calculate the net fractional Kuhn bond orientation and the reformulated expression for the decrease in the friction coefficient due to net Kuhn relative bond alignment of the test chain with respect to the matrix chains. Note here that structural parameters of PS are used since the experimental data of PS melts and solutions are compared with the predictions by various models studied in this paper.

We start by denoting the net Kuhn bond orientation in the polydisperse MLD toy model single segment as $\mathbf{S}_{Kuhn}$. The net Kuhn bond orientation of the matrix is proportional to the birefringence which, using the freely jointed chain model in a Kuhn–Grün analysis, yields

$$\mathbf{S}_{Kuhn} = \left(1 - \frac{3x}{\mathrm{L}^{-1}(x)}\right)\mathbf{S}_{tube} + isotropic\ terms = \left(1 - \frac{3x}{\mathrm{L}^{-1}(x)}\right)\langle \widehat{R}\,\widehat{R}\,\rangle + isotropic\ terms, \tag{8}$$

where $\mathbf{S}_{tube}$ is the single tube segment orientation. The inverse Langevin function term, $\mathrm{L}^{-1}(x)$, in Eq. (8) can be accurately approximated within 1% [Treloar (1975), p. 178] for easy calculation

$$\left(1 - \frac{3x}{\mathrm{L}^{-1}(x)}\right) \approx \frac{3}{5}x^2 + \frac{1}{5}x^4 + \frac{1}{5}x^6, \tag{9}$$

where x is the fractional chain extension

$$x \equiv \frac{\lambda}{\lambda_{\max}}. \tag{10}$$

Note here that Yaoita *et al.* (2012) use the simplest approximation $\{1 - [3x/\mathrm{L}^{-1}(x)]\} \approx x^2$ in their work. It is also noted that the definition of x will be altered, $x \equiv (\Lambda/\Lambda_{\max})$, for models that include entanglement density dynamics.

The maximum relative stretch $\lambda_{\max}$ is calculated as [Mead (2011b)]

$$\lambda_{\max} = n^{1/2} = 0.82\left[\frac{M_e}{C_\infty M_0}J\right]^{1/2}. \tag{11}$$

Here, J is the number of carbon-carbon sigma bonds in the backbone, $J = 2$ for PS, M_e is the equilibrium average entanglement molecular weight (13 333 Da for PS). In nonequilibrium flow situations, the entanglement molecular weight is a function of concentration and the dynamic entanglement density along the chain. C_∞ is the characteristic ratio, 9.8 for PS [Flory (1969)] and M_0 is the monomer molecular weight, 104 Da for PS. n is the number of Kuhn bonds in an entanglement segment. Note that for PS melts $\lambda_{\max} = 4.2$, a relatively small maximum stretch. The maximum stretch will be much larger ($\lambda_{\max} > 25$) for the entangled high molecular weight (MW) entangled PS solutions considered by Bhattacharjee *et al.* (2002).

Ianniruberto *et al.* calculated the functional form of the reduced friction versus matrix Kuhn bond orientation for monodisperse PS melts in their 2012 paper [Ianniruberto *et al.* (2012), see Fig. 4]. We use the Ianniruberto *et al.* (2012) CDFC calculation as a guide

$$\frac{\varsigma(t)}{\varsigma_{eq}} = \frac{\tau_{d,0}(t)}{\tau_{d,eq}} = \frac{\tau_s(t)}{\tau_{s,eq}} = 0.02239(S_{Kuhn}(t))^{-1.65} \quad S_{Kuhn} > 0.1, \tag{12}$$

where ς is the monomeric friction coefficient, τ_d is the reptation time, and τ_s is the longest Rouse relaxation time. Subscript "*eq*" indicates equilibrium value and "0" means a value for a fully entangled chain.

The true form of the dependence of the accelerated relaxation rate can in principle be determined by the nonlinear extensional stress relaxation experiments of Yaoita *et al.* (2012) which are of fundamental importance with respect to CDFC. These experiments are discussed in detail in Sec. VI and Fig. 7.

Following Yaoita *et al.* (2012), we define the scalar net fractional Kuhn bond alignment S_{Kuhn} as

$$S_{Kuhn} \approx \phi_p \left(\frac{3}{5}x^2 + \frac{1}{5}x^4 + \frac{1}{5}x^6 \right) |\mathbf{S}_{tube}| \tag{13}$$

The fractional Kuhn bond orientation, S_{Kuhn}, varies between zero and one for perfect orientation. The anisotropic tube orientation in uniaxial extension is denoted by $|\mathbf{S}_{tube}| = (S_{xx} - S_{yy})$. For shear deformation, the principal values must be used, $|\mathbf{S}_{tube}| = [(S_{xx} - S_{yy})^2 + 4S_{xy}^2]^{1/2}$. The mass fraction of polymer scales the fractional Kuhn bond orientation and is represented by ϕ_p such that CDFC for both melts, $\phi_p = 1$, and entangled solutions, $\phi_p < 1$, can be modelled.

III. MODIFICATION OF THE DESAI–LARSON TOY DEMG MODEL TO INCORPORATE ED, CDFC, AND CCR

Here, we briefly outline how to incorporate the new results in Secs. II and II A into the Desai–Larson modified DEMG model [Desai and Larson (2014)]. We eliminate the Desai and Larson tube dilation effect and replace it with the CDFC and EDs results presented in Secs. II and II A above. This allows *both* the disengagement time and the stretch time to be modified by CDFC which should in principle allow an accurate modeling of steady state extensional viscosity data for *both* melts and solutions.

One of the key theoretical developments in the Desai–Larson model is the derivation of a new stretch dynamics equation for the partially disentangled chain that incorporates the fact that the maximum extension is a function of the entanglement density [Mead (2011b)]. When $M_e(t) = [M/N(t)]$ changes (increases) with deformation induced disentanglement, the maximum stretch also increases as described below

$$\Lambda_{\max}(t) = n^{1/2} = 0.82\left[\frac{M_e(t)}{C_\infty M_0}J\right]^{1/2} = 0.82\left[\frac{M}{C_\infty M_0 N(t)}J\right]^{1/2}. \tag{14}$$

There is one new stretching effect to account for in the stretch equation: Stretch shortening due to removal of chain back folds. The stretch dynamical equation for the diluted (partially disentangled) chain, generalized to include CR effects, is [Desai and Larson (2014), Mead *et al*. (1998)]

$$\dot{\Lambda}(t) = \underbrace{-\left[\frac{\dot{\alpha}(t)}{\alpha}\Lambda\right]}_{\substack{\text{stretch reduction} \\ \text{due to disentanglement}}} + \underbrace{(\boldsymbol{\kappa} : \mathbf{S}_{tube})\Lambda}_{\text{affine stretch}} - \underbrace{k_s\left(\frac{\Lambda - 1}{\tau_s}\right)}_{\text{chain retraction}}$$
$$\underbrace{-\frac{1}{2}(\Lambda - 1)\left[\boldsymbol{\kappa} : \mathbf{S}_{tube} - \frac{\dot{\Lambda}}{\Lambda} + \frac{\dot{\alpha}(t)}{\alpha} + \frac{1}{\Lambda^2 \tau^1{}_d(t)}\right]}_{\text{CCR driven tube shortening}}, \tag{15}$$

where

$$\alpha(t) = \frac{\Lambda_{\max}(t)}{\lambda_{\max}} = \left[\frac{N_e}{N(t)}\right]^{1/2} \quad \text{and} \quad \dot{\alpha}(t) = -\frac{1}{2}[N_e]^{1/2}[N(t)]^{-3/2}\dot{N}(t), \tag{16}$$

and the nonlinearity of the spring is incorporated in a single factor denoted by k_s [Cohen (1991); Desai and Larson (2014)]

$$k_s(t) \equiv \frac{\mathrm{L}^{-1}\left(\dfrac{\Lambda(t)}{\Lambda_{\max}(t)}\right)}{3\dfrac{\Lambda(t)}{\Lambda_{\max}(t)}} \approx \frac{\left(3\lambda_{\max}^2\alpha^2-\Lambda^2\right)/\left(\lambda_{\max}^2\alpha^2-\Lambda^2\right)}{\left(3\lambda_{\max}^2\alpha^2-1\right)/\left(\lambda_{\max}^2\alpha^2-1\right)}. \tag{17}$$

We have added a CCR tube shortening term to the Desai–Larson stretch equation (15) that requires discussion. This is done in Sec. IV below.

The above generalized expression of the stretch dynamics is principally what we take from the Desai–Larson diluted tube model. We use the EDs model presented in Sec. II to replace the tube dilation dynamics expressions in the Desai–Larson model.

IV. MODIFICATION OF THE NEW CDFC-ED TOY MLD MODEL TO ACCOUNT FOR REDUCED LEVELS OF CCR FOR HIGHLY ALIGNED SYSTEMS

In this section, we outline the manner in which the previously presented model can be modified to account for the idea that CCR effects are different (greatly reduced) in systems of slightly oriented versus highly oriented chains. These effects will impact CCR driven reorientation as well as CCR driven stretch relaxation (tube shortening) in fast flows [Mead *et al*. (1998)]. These ideas are partly motivated by the work of Desai and Larson (2014) that showed that CCR appears not to be important to capture the salient features of fast nonlinear extensional flows. This is a conclusion that we affirm in calculations with our new model.

The specific effect, we wish to incorporate in our model, is that CCR effects do not strongly impact highly aligned chains. For example, in the limit of perfectly aligned chains in fast flow, there are no dynamical (topological) constraints and consequently CCR will have no effect on the orientation or stretch of the test chain even though $\boldsymbol{\kappa} : \mathbf{S}_{tube}$ is very large [Desai and Larson (2014)]. Of course, this ideal limiting situation can only be approached in any finite deformation rate flow. We propose an *ad hoc* empiricism that smoothly transits between the Gaussian and highly oriented extreme situations. A sketch of these ideas for CCR driven stretch relaxation is shown in Figs. 1 and 2.

We propose the following empirical changes to the stretch and orientation dynamical equations to account for the ideas presented in the above thought experiment. CCR in stretching flows relaxes $(1/2)(\Lambda-1)$ of the stretch associated with a given entanglement [Mead (2011a)]. Using the above ideas, we construct an empirical function that smoothly transits between the Gaussian and highly oriented cases

$$\underbrace{\frac{1}{2}(\Lambda-1)}_{\substack{\textit{Gaussian tube}\\ \textit{shortening}}} \underbrace{-\frac{1}{2}(|\mathbf{S}_{tube}|)(\Lambda-1)}_{\substack{\textit{highly oriented biased}\\ \textit{tube shortening}}} = \frac{1}{2}(1-|\mathbf{S}_{tube}|)(\Lambda-1). \tag{18}$$

We have included a new empirical term to the tube shortening expression, $(1-|\mathbf{S}_{tube}|)$. Figure 1 illustrates the physical ideas underlying this empirical factor multiplying the tube shortening term. Note that for $|\mathbf{S}_{tube}| \approx 1$, we assume the chain is unraveled and linear rather than a zig-zagged cat's cradle (back folded) conformation. The new term effectively wipes out tube shortening stretch relaxation for fast flows where the tube is highly oriented. Desai and Larson (2014) have shown that this is a desirable feature to have in the model for fast uniaxial extension and this underlies the motivation for this *ad hoc* factor in the stretch equation.

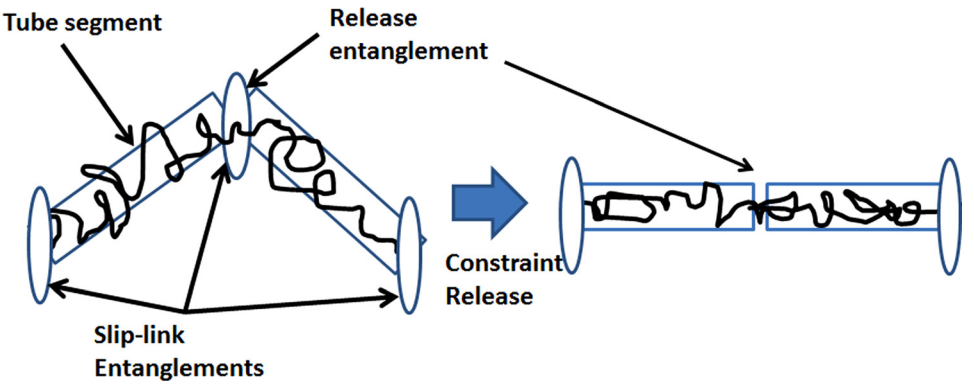

FIG. 1. Schematic diagram for tube shortening when $|\mathbf{S}_{tube}| < 1$: The tube is crinkled and constraint release shortens the tube and relaxes stretch and orientation [Mead *et al.* (1998); Mead (2011a)].

Incorporating the new proposed physics into the stretch equation yields

$$\dot{\Lambda}(t) = -\left[\frac{\Lambda}{\alpha}\dot{\alpha}(t)\right] + (\boldsymbol{\kappa} : \mathbf{S}_{tube})\Lambda - k_s\left(\frac{\Lambda - 1}{\tau_s}\right) - \frac{1}{2}(1 - |\mathbf{S}_{tube}|)(\Lambda - 1)\left[\boldsymbol{\kappa} : \mathbf{S}_{tube} - \frac{\dot{\Lambda}}{\Lambda} + \frac{\dot{\alpha}(t)}{\alpha} + \frac{1}{\Lambda^2\tau^1{}_d(t)}\right]. \tag{19}$$

Thus, at high fractional extensions the effect of CCR on stretch smoothly disappears as $|\mathbf{S}_{tube}|$ monotonically increases. Thus, CCR can effectively reduce stretch in shear flows where the orientation is lower than it is in extensional flows.

We also propose an *ad hoc* modification to the orientation dynamics equation to account for biased (reduced) reorientation due to nematic (molecular packing) effects in highly aligned systems. Nematic effects are well established in cross-linked rubbers and polymer melts [Doi *et al.* (1989)]. In such highly oriented systems the switch function, $(1/\Lambda)$, already diminishes the effect of CCR on the reorientation process. We add to this effect with an *ad hoc* empirical nematic reorientation suppression factor $(1 - S_{Kuhn})$

$$\frac{1}{\tau(t)} = (1 - S_{Kuhn})\left[\frac{1}{\Lambda^2(t)\tau^1{}_d(t)} + \frac{1}{\Lambda}\left[\boldsymbol{\kappa} : \mathbf{S}_{tube} - \frac{\dot{\Lambda}}{\Lambda} + \frac{\dot{\alpha}(t)}{\alpha} + \frac{1}{\Lambda^2\tau^1{}_d(t)}\right]\right]. \tag{20}$$

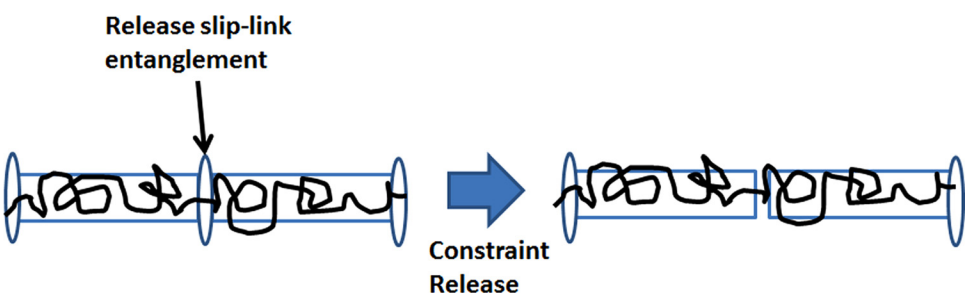

FIG. 2. Schematic diagram for tube shortening when $|\mathbf{S}_{tube}| \approx 1$: Constraint release does not relax any stretch. Note that the tube is unraveled and linear rather than in a zig-zag cat's cradle (back folded) conformation ($|\mathbf{S}_{tube}| \approx 1$ in both cases). Fast, large deformations unravel the chain and generate highly extended nearly linear conformations [Desai and Larson (2014), see Fig. 1].

The factor $(1 - S_{Kuhn})$ empirically accounts for the idea that the reorientation process will be biased (reduced) by nematic packing effects due to the net Kuhn bond orientation of the matrix. Note that we are actually not including a biased reorientation but rather an increased orientational relaxation time which has a similar effect on the orientation level. Another way to look at this effect is that CR effects will be ineffectual in highly aligned systems, i.e., when S_{Kuhn} is large (see Figs. 1 and 2). Including the new factor of $(1 - S_{Kuhn})$ along with the switch function will effectively reduce all CCR driven reorientation in fast stretching flows where S_{Kuhn} is large.

Note that there will be a sharp distinction between uniaxial extension and shear with the above two modifications. In uniaxial extension, the orientation and stretch is severe and the above two modifications will both kick in. Conversely, in shear flows the orientation and stretch is weak and $(1 - S_{Kuhn}) \approx 1$ such that there are no nematic effects in melts or solutions.

V. SUMMARY OF THE EQUATIONS IN THE EDS—KUHN BOND CDFC REFORMULATION OF THE MONODISPERSE MLD TOY MODEL

Here, we briefly summarize the equation set for the new monodisperse MLD "toy" model [see Desai and Larson (2014), Eqs. (31)–(37) and note the differences]. We are only considering the monodisperse case here. Generalizing the results to polydisperse systems is an important goal of this work. This is straightforward and is done in Appendix B.

We start with the deterministic differential evolution equation for the entanglement pair orientation, $\mathbf{S}_{tube}$ [Desai and Larson (2014); Mead (2007); Larson (1984); Marrucci (1984)]. We choose the differential approximation to the orientation evolution for coding simplicity and speed in computing. Here, $\hat{\mathbf{S}}_{tube}$ represents the upper convected time derivative

$$\hat{\mathbf{S}}_{tube}(t) + 2(\boldsymbol{\kappa}(t) : \mathbf{S}_{tube}(t))\mathbf{S}_{tube} + \left(\frac{1 - S_{Kuhn}}{\tau(t)}\right)\left(\mathbf{S}_{tube}(t) - \frac{1}{3}\boldsymbol{\delta}\right) = 0. \tag{21}$$

Relaxation time

$$\frac{1}{\tau(t)} = \frac{1}{\Lambda^2(t)\tau^1{}_d(t)} + \left(\frac{1}{\Lambda}\right)\left[\boldsymbol{\kappa} : \mathbf{S}_{tube} - \frac{\dot{\Lambda}}{\Lambda} + \frac{\dot{\alpha}(t)}{\alpha} + \frac{1}{\Lambda^2\tau^1{}_d(t)}\right], \tag{22}$$

where

$$\tau^1{}_d(t) = \left(\frac{N(t)}{N_e}\right)\tau_{d,0}(t) \tag{23}$$

and CDFC

$$\frac{\varsigma(t)}{\varsigma_{eq}} = \frac{\tau_{d,0}(t)}{\tau_{d,eq}} = \frac{\tau_s(t)}{\tau_{s,eq}} = 0.02239(S_{Kuhn}(t))^{-1.65} \quad S_{Kuhn} > 0.1, \tag{24}$$

$$S_{Kuhn} = \phi_p\left(1 - \frac{3x_i}{\mathrm{L}^{-1}(x_i)}\right)|\mathbf{S}_{tube}| \approx \phi_p\left(\frac{3}{5}x^2 + \frac{1}{5}x^4 + \frac{1}{5}x^6\right)|\mathbf{S}_{tube}|, \tag{25}$$

where $x \equiv (\Lambda/\Lambda_{\max})$ and for uniaxial stretch $|\mathbf{S}_{tube}| = (S_{xx} - S_{yy})$ while for shear deformation

$$|\mathbf{S}_{tube}| = \left[(S_{xx} - S_{yy})^2 + 4S_{xy}^2\right]^{1/2}. \tag{26}$$

EDs

$$\dot{N}(t) = \frac{2N_e}{\tau_{d,o}(t)}\left[\frac{N_e}{N(t)} - 1\right] - \beta\left[\boldsymbol{\kappa} : \mathbf{S}_{tube} - \frac{\dot{\Lambda}}{\Lambda} + \frac{\dot{\alpha}(t)}{\alpha}\right]N(t). \tag{27}$$

Stretch dynamics

$$\dot{\Lambda}(t) = -\left[\frac{\Lambda}{\alpha}\dot{\alpha}(t)\right] + (\boldsymbol{\kappa} : \mathbf{S}_{tube})\Lambda - k_s\left(\frac{\Lambda - 1}{\tau_s}\right) - \frac{1}{2}(1 - |\mathbf{S}_{tube}|)(\Lambda - 1)\left[\boldsymbol{\kappa} : \mathbf{S}_{tube} - \frac{\dot{\Lambda}}{\Lambda} + \frac{\dot{\alpha}(t)}{\alpha} + \frac{1}{\Lambda^2\tau^1{}_d(t)}\right], \tag{28}$$

$$\alpha(t) \equiv \frac{\Lambda_{\max}(t)}{\lambda_{\max}} = \left[\frac{N_e}{N(t)}\right]^{1/2} \quad \text{and} \quad \dot{\alpha}_i(t) = -\frac{1}{2}[N_e]^{1/2}[N(t)]^{-3/2}\dot{N}(t). \tag{29}$$

Nonlinear spring

$$k_s(t) \equiv \frac{\mathrm{L}^{-1}\left(\dfrac{\Lambda(t)}{\Lambda_{\max}(t)}\right)}{3\dfrac{\Lambda(t)}{\Lambda_{\max}(t)}} \approx \frac{\left(3\lambda_{\max}^2\alpha^2 - \Lambda^2\right)/\left(\lambda_{\max}^2\alpha^2 - \Lambda^2\right)}{\left(3\lambda_{\max}^2\alpha^2 - 1\right)/\left(\lambda_{\max}^2\alpha^2 - 1\right)}. \tag{30}$$

Stress calculator

$$\boldsymbol{\sigma}(t) = 3G_N(t)\left[\frac{\mathrm{L}^{-1}\left(\dfrac{\Lambda(t)}{\Lambda_{\max}(t)}\right)}{3\dfrac{\Lambda(t)}{\Lambda_{\max}(t)}}\right]\Lambda^2\mathbf{S}_{tube} \approx 3G_N(t)\,k_s(t)\,\Lambda^2(t)\,\mathbf{S}_{tube}(t), \tag{31}$$

where the partially disentangled modulus is defined as

$$G_N(t) \equiv \frac{\rho RT}{\left(\dfrac{M}{N(t)}\right)} = \frac{N(t)}{N_e}G_N^0. \tag{32}$$

The fact that the modulus is a function of time, $G_N(t) = [N(t)/N_e]G_N^0$, clearly demonstrates that the new model will predict shear modification. For high molecular weight systems or systems with LCB, the entanglement microstructure will take an extended time to heal during which the measured dynamic moduli will be lower than their equilibrium values, $G^*(\omega, t) < G^*(\omega, \infty)$. This shear modification can be quite large and last for an extended period of time as the entanglement microstructure slowly heals via the diffusive process of reptation [Rastogi *et al.* (2003); Rokudai (1979)]. The entanglement

TABLE I. Summary of the family of toy molecular models studied.

Model	CCR	ED	CDFC
DEMG	off	off ($\beta = 0$)	Off
DEMG-cdfc	off	off ($\beta = 0$)	On
MLD	on	off ($\beta = 0$)	Off
MBP	on	on ($\beta \neq 0$)	On
MBP-xccr	off	on ($\beta \neq 0$)	On

microstructure will heal on a time scale of the disengagement time, $\tau_{d,0}$, which can be very long indeed for high molecular weight or LCB systems.

VI. SIMULATION OF MONODISPERSE LINEAR PS MELTS AND ENTANGLED SEMIDILUTE SOLUTIONS IN STEADY AND TRANSIENT UNIAXIAL EXTENSION

In this section, we explore the properties of the new MBP EDs model for monodisperse systems by numerically solving the system of Eqs. (21)–(32) summarized in Sec. V. Although the equation set appears complex and formidable, they are all ordinary differential equations that can be stepped forward in time using the simple Euler method. Because the Euler method is first order in time care must be taken to take small enough time step sizes to ensure convergence. Using the Euler method makes the code simple to write and fast to execute. Computational speed becomes an issue when polydispersity is introduced particularly so when the integral form of the orientation evolution equation is used [Mishler and Mead (2013a, 2013b)].

We will execute our study by including/excluding various physical effects to isolate their significance. The physics we are interested in understanding are CCR, ED (through β), and CDFC. The simulation software allows us to turn the specific physics "on"/"off" and to thereby quantify the impact of the specific physics on rheology. We shall be particularly interested in the following basic models summarized in Table I. The experimental data sets, which are used to compare with the calculated prediction results, are summarized in Table II.

The first simulations we perform are for the flow curves for steady uniaxial extension of monodisperse PS melts. For these simulations, we shall choose a value of $\beta = 0.12$ (ED on) in Eq. (27). This value is chosen such that the shear stress-shear rate curve is monotonic (see Fig. 10 of Sec. VI A). A monotonic shear stress-shear rate curve is necessary for stable shear flow [Ianniruberto and Marrucci (2001)]. All values of $\beta < 0.12$ yield monotonic shear stress-shear rate curves.

TABLE II. Experimental data sets compared (input parameter estimations were referred to Desai and Larson (2014) and Likhtman and McLeish (2002). $M_e = 13\,333$ Da is used for all PS melts to give $\lambda_{max} = 4.2$ whereas M_e for solutions are evaluated by dividing by $\Phi_p^{1.2}$. The values of $\tau_{d,f}$ given below include the effect of double reptation.)

Sample	G_N^0 (kPa)	$\tau_{d,f}$ (s)	$\tau_{S,eq}$ (s)	N_{eq}	Ref.
PS200K	200	1610	94.3	15	Bach *et al.* (2003)
PS200K-S	200	1.33	0.065	15	Schweizer *et al.* (2004)
PS545K	250	54418	779	41	Huang *et al.* (2013)
PS145K	290	7839	1134	10.7	Yaoita *et al.* (2012)
20% 1.95 M PS	6.8	6.26	0.17	30.4	Acharya *et al.* (2008)
7% 8.42 M PS	0.52	31.65	0.6	44.3	Pattamaprom and Larson (2001)

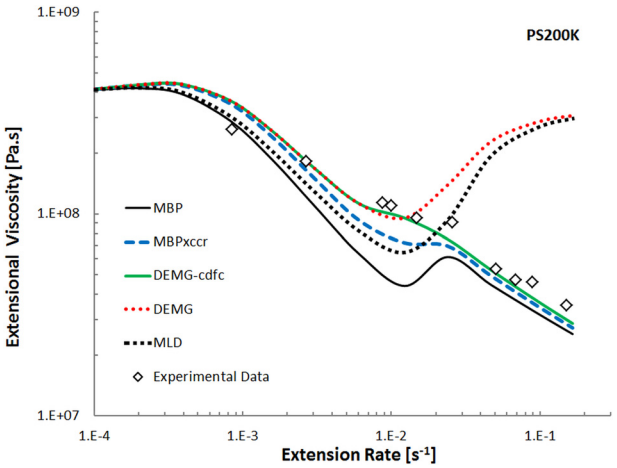

FIG. 3. Steady state extensional viscosity as a function of extension rate: Experimental data are for monodisperse PS200K at 130 °C [Bach *et al.* (2003)]. Predictions are from various options of the family of models (see figure legend and Table I). This allows us to determine that CDFC is the essential ingredient required to capture the monotonic extensional flow curve of monodisperse PS melts. The kink in the MBP flow curve begins at $\dot{\varepsilon}\tau_{s,eq} \approx 1$.

The first system we shall study is PS200K [130 °C monodisperse PS melt by the work of Bach *et al.* (2003)] in steady state extensional flow. The average equilibrium number of entanglements per chain in this system is 15. The results of a variety of simulations are shown in Fig. 3 along with the experimental data. The base case for comparison is the DEMG model which has no ED, CCR, or CDFC. The DEMG line in Fig. 3 shows a ladle shaped flow curve. The upturn in viscosity is associated with the onset of chain stretching and occurs when the stretch Weissenberg number is about unity, $\dot{\varepsilon}\tau_{s,eq} \approx 1$. Complimentary to the DEMG model is the MLD toy model which is simply the DEMG model with CCR switched on. Here again, we see the ladle shaped flow curve, lowered relative to the DEMG model by the additional relaxation mechanism of CCR. The predicted flow curves of both the DEMG and MLD models are qualitatively and quantitatively at odds with the experimental data.

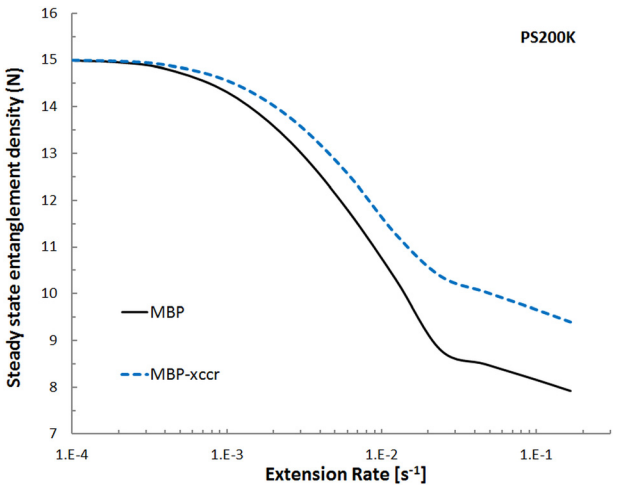

FIG. 4. The steady state entanglement density, $N(\dot{\varepsilon})$, versus extension rate, $\dot{\varepsilon}$, for the MBP model and the MBP-xccr model. The system simulated is monodisperse PS200K at 130 °C. For the case where ED is turned off, i.e., DEMG-CDFC the entanglement density is a *constant* equal to the equilibrium value of 15 (data not shown).

The next simulation we execute is the base DEMG model with CDFC now turned on (DEMG-cdfc). Its flow curve is now monotonic extension thinning and closely mimics the experimental data both before and after $\dot{\varepsilon} \approx (1/\tau_{s,eq})$. This result, and those presented in what follows, strongly suggest that CDFC is the essential feature needed to achieve a monotonic thinning extensional flow curve for monodisperse PS melts [Desai and Larson (2014)].

The simulation results are sensitive to the details of the specific expression for CDFC used. In particular, the details of the form of the expression for S_{Kuhn} used matter in the simulations. The shape of the flow curve is determined by the specific functional form of CDFC used [see Eqs. (24)–(26)]. In particular, to achieve a monotonic flow curve CDFC must be activated slightly before $\dot{\varepsilon} \approx (1/\tau_{s,eq})$. If CDFC is activated later than $\dot{\varepsilon} \approx (1/\tau_{s,eq})$, a "kink" will occur in the flow curve. Precisely, when CDFC is activated depends on the specific functional form of the CDFC we use.

The next simulation we perform is to include ED in the simulation. In this case, we choose $\beta = 0.12$ with both CCR on and CDFC on, i.e., the MBP model. ED is on for any $1 > \beta > 0$. This generates the black solid curve in Fig. 3. Here, for $\dot{\varepsilon} < (1/\tau_{s,eq})$, we observe excessive thinning with lower viscosity values relative to those for DEMG-cdfc which is caused by CCR. The curve also shows an upturn around $\dot{\varepsilon} \approx (1/\tau_{s,eq})$ due to the onset of stretch. However, for $\dot{\varepsilon} > (1/\tau_{s,eq})$, it becomes a thinning curve again, approximately parallel to the DEMG-cdfc case. This thinning effect is due to the effects of CDFC being activated. Hence, the results especially at $\dot{\varepsilon} > (1/\tau_{s,eq})$ are approximately *equivalent* to the DEMG-cdfc model when we add ED despite the fact that the internal workings of the two models are entirely *different*. In particular the average number of entanglements is dramatically lower when ED is turned on resulting in a lower modulus. The lower modulus implies a different entanglement microstructure relative to the DEMG model with CDFC now turned on which predicts a constant entanglement density.

The final simulation we perform is with $\beta = 0.12$, ED on, CCR off, and CDFC on (MBP-xccr). This is shown as the blue dashed line curve in Fig. 3. As with the DEMG-cdfc model, the MBP-xccr model generates results very close to the experimental data. The flow curve shows a much smaller kink right after $\dot{\varepsilon} \approx (1/\tau_{s,eq})$ than that of the MBP curve and closely mimics the experimental data. The small kink is the result of stretch being activated prior to CDFC being activated. Choosing a different functional form for CDFC can in principle eliminate this kink by modifying precisely when CDFC is activated relative to $\dot{\varepsilon} \approx (1/\tau_{s,eq})$. Precisely when CDFC is activated is impacted by whether ED and CCR are on or off. The details of the models, including when CDFC is activated, are displayed in the figures of Appendix C.

We now address the perplexing question of why the simulations of the "straight" DEMG-cdfc are very similar to the new MBP-xccr model with $\beta = 0.12$, i.e., although the details of the two models, such as the number of entanglements and the modulus, are profoundly different, they nevertheless yield approximately equivalent extensional flow curves in close agreement with experimental data. Figure 4 plots the average number of entanglements per chain versus extension rate for $\beta = 0.12$ with CCR off and CDFC on (MBP-xccr model). We see that for fast extensional flows the average number of entanglements per chain is approximately half that at equilibrium. Physically, the modulus is the manifestation of the entanglement microstructure [see Eq. (32)] and hence the modulus drops off proportionately. Thus, the new MBP-xccr model predicts significant changes in the entanglement microstructure in fast extensional flow.

Figure 5 plots the steady state relative stretches, λ and Λ, for the two different models (DEMG-cdfc and MBP-xccr) versus extension rate. Clearly the relative stretch of the

MBP simulations, Λ, is significantly larger than the relative stretch of the DEMG-cdfc simulation, λ. The reason that these two simulations yield approximately equivalent extensional flow curves is that the effect of ED on the modulus, Eq. (32), is effectively canceled by the corresponding increase in stretch. Using the expression for the stress (31), we argue that for the two models the following products are proportional to the extensional stress and are approximately equal even though $\Lambda \neq \lambda$

$$G_N(t)\Lambda^2_{MBPxccr}(t) \approx G^0_N \lambda^2_{DEMGcdfc}(t). \tag{33}$$

Here, we have made the assumption that orientation has effectively saturated when stretch commences. The saturated orientation cancels on both sides of Eq. (33). We have also assumed that the non-Gaussian factors k_s are both close to unity and cancel. Note that for any given model with ED the following equality holds:

$$G_N(t)\Lambda^2_{ED}(t) = G^0_N \left(\frac{N(t)}{N_e}\right) \lambda^2_{ED}(t) \left(\frac{N_e}{N(t)}\right) = G^0_N \lambda^2_{ED}(t). \tag{34}$$

Here, $\lambda^2_{ED}(t)$ represents the stretch relative to the equilibrium extension in any model with ED. Hence, another way to see the approximation in Eq. (33) is to note that both the DEMG-cdfc and MBP-xccr models yield similar expressions for the extensional stress in fast steady extension, Eq. (34). However, note that $\lambda^2_{ED}(t)$ and $\lambda^2_{DEMG}(t)$ are calculated differently in each model and hence are *not* equal.

The argument underlying Eq. (33) may very well explain the apparent "success" of the mono and polydisperse MLD models in predicting nonlinear flows despite the fact that all MLD models assume a *constant* entanglement density [Mead (1998, 2011a); Mishler and Mead (2013a, 2013b)].

In Fig. 6, we examine the transient extensional viscosity versus time for the PS200K melt. Transient extensional viscosities are more typical of what one encounters in practice since steady state (Hencky strains greater than $\sim$3) extensional viscosities are very

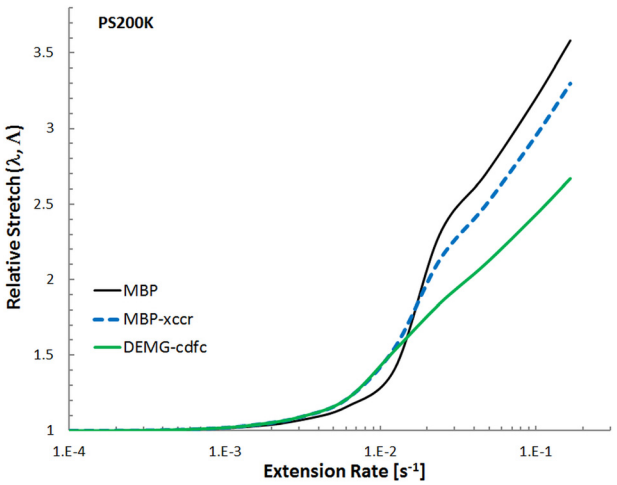

FIG. 5. The relative stretches for MBP, MBP-xccr, and DEMG-cdfc The respective curves are: $\lambda(\dot{\varepsilon})$ vs $\dot{\varepsilon}$ (DEMG-cdfc) and $\Lambda(\dot{\varepsilon})$ vs $\dot{\varepsilon}$ (MBP and MBP-xccr) for the monodisperse PS200K melt. The relative stretch $\Lambda(\dot{\varepsilon})$ is *increased* relative to the base DEMG-cdfc case by virtue of the unraveling of back folds that occurs in the new model [Desai and Larson (2014)].

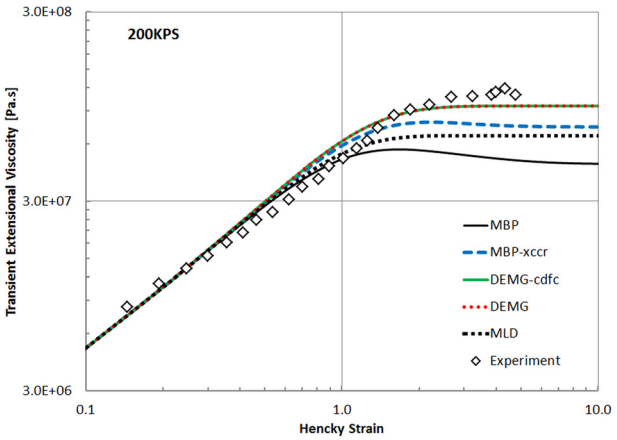

FIG. 6. Transient extensional viscosity, $\eta_e(t)$ versus t, for monodisperse PS200K at an extension rate of $0.01\,s^{-1}$ ($\dot{\varepsilon}\tau_{s,eq} \approx 1$). Note the small and broad maximum in the transient viscosity at a Hencky strain of ~ 1.5 for the MBP model. This is caused because ED lags the stress, i.e., it takes many Hencky strain units to partially disentangle the melt. Note that the results from the DEMG and DEMG-cdfc models are effectively on top of each other since this extension rate is below the onset of CDFC threshold.

difficult to achieve experimentally. The specific case that we examine is for an extension rate of $0.01\,s^{-1}$ which corresponds to a stretch Weissenberg number of $\dot{\varepsilon}\tau_{s,eq} \approx 1$. Note the broad maximum in the MBP curve at a Hencky strain of $\sim$1.5. The cause of the maximum is that EDs $[N(t)]$ is controlled by ED and lags the stress, only slowly approaching its steady state value. As in the case for the steady uniaxial flow curves, the DEMG-cdfc and MBP-xccr models provide the best fit to the data.

The next transient extensional experiment we examine is stress relaxation after imposing three Hencky strain units on a PS145K at 120 °C. These experiments were performed by Yaoita *et al.* (2012) and provide definitive, hard experimental evidence for the existence of CDFC. Figure 7 displays the results of our simulations along with the experimental data. Figure 7 experimentally demonstrates that CDFC accelerates the relaxation following

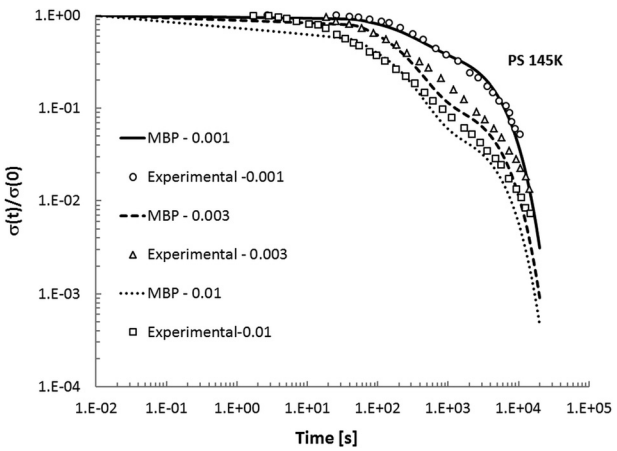

FIG. 7. Normalized stress relaxation after imposing three Hencky strain units for a monodisperse PS145K melt at 120 °C at three different steady extension rates. The higher the extension rate, the higher the net Kuhn bond orientation and the greater the effect of CDFC on the initial rate of stress relaxation. The MBP model captures this effect.

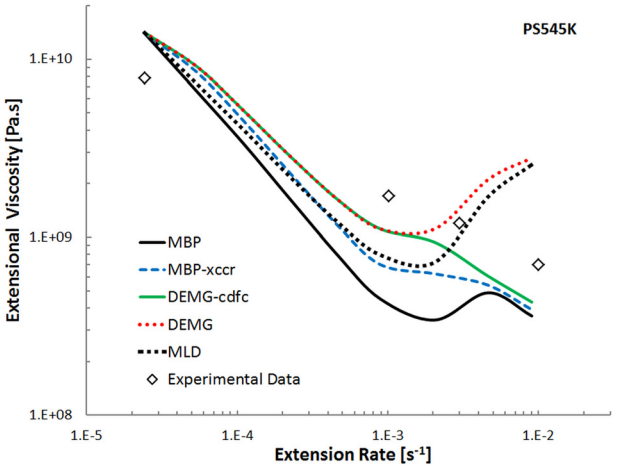

FIG. 8. Steady state extensional viscosity as a function of extension rate. Experimental data are for monodisperse PS545K melt at 130 °C [Huang *et al.* (2013)]. Predictions are from various options of the family of models (see figure legend and Table I). Once again the DEMG-CDFC and MBPxccr models perform best.

cessation of stretch. The higher the initial stress, the higher the net Kuhn bond orientation and the larger the CDFC effect and hence the faster the initial relaxation rate. The systematic increase in the initial rate of relaxation strongly supports the existence of CDFC and this effect is quantitatively captured in the MBP model. Additionally, for the MBP model, the entanglement density relaxes on a time scale of $\tau_d \approx 7800$ s, much slower than the time scale shown in Fig. 7. Hence, the modulus is lowered relative to the equilibrium state and persists even though the deformation has ceased and this effect does not impact the relaxation processes in Fig. 7. This phenomenon is shear modification.

Finally, we examine another PS melt, PS545k studied by Huang *et al.* (2013). The principal difference between this set of experiments/simulations and Fig. 3 is that the average number of entanglements per chain is very large, $Z \sim 41$. Hence, the separation between the equilibrium stretch and orientational relaxation times is correspondingly large since $\tau_d \approx 3Z\tau_s$. However, despite this distinction the salient features of Fig. 8 are largely similar to those discussed for the PS200K melt in Fig. 3. In particular, we see an enhanced sensitivity as to precisely when CDFC is activated relative to the onset of stretch. This sensitivity manifests itself in the size of the kink in the flow curve as discussed above with respect to Fig. 3. These simulations provide a severe test for the precise functional form of CDFC used.

Figure 9 shows the steady state experimental extensional flow curves for 20 wt. % 1.95 M PS solution at 21 °C showing monotonic thinning before, and hardening after, $\dot{\varepsilon}\tau_{s,eq} \approx 1$ [Acharya *et al.* (2008)]. The new MBP model qualitatively captures the salient ladle shape features of the flow curve data as does the straight DEMG model without ED, CDFC, or CCR. Once again, the DEMG-cdfc and MBP-xccr provide the best fits to the experimental data.

Thus the new MBP-xccr model, which includes ED and CDFC, captures *both* the monotonic thinning behavior of monodisperse PS melts and the thinning/hardening behavior observed for entangled PS solutions. For solutions, CDFC is effectively diluted out and is ineffective due to the factor of ϕ_p in Eq. (13) a point which is also discussed by Yaoita *et al.* (2012). Hence, the results from the DEMG and DEMG-cdfc models are almost identical since CDFC is diluted out and is essentially inactive in semidilute solutions.

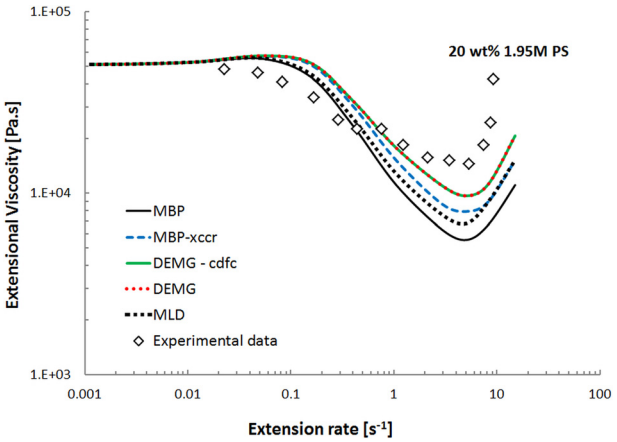

FIG. 9. Steady state extensional viscosity as a function of extension rate. Experimental data are for a monodisperse 20% 1.95 M PS solutions at 21 °C [Acharya *et al*. (2008)]. Predictions are from various options of the family of models (see figure legend and Table I). Note that the results from DEMG and DEMG-cdfc are on top of each other.

A. Simulation of monodisperse linear PS melts and solutions in steady and transient shear flow

Since we are interested in a generally applicable toy molecular model, we examine the predictions of the new MBP model in steady and transient shear flow. Here, the orientations will be lower than in fast extensional flows and we anticipate that CCR will be more important than it is in fast extensional flows.

The first issue we address is determining the range of allowable values for β. We do this by demanding that the shear stress vs shear rate curve be monotonic such that, consistent with most experiments, shear flow of melts is stable [McLeish and Ball (1986)]. Figure 10 displays the derivative of several shear stress vs shear rate curves for different values of β. It is evident that the shear stress-shear rate curves are monotonic (all positive slopes) for all $\beta < 0.12$ and exhibit a broad maximum for $\beta > 0.12$. Hence, for our simulations, we choose the maximum allowable value for $\beta = 0.12$.

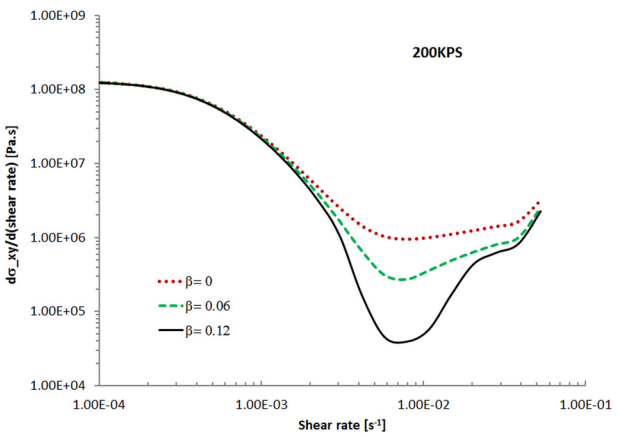

FIG. 10. The (slope of shear stress-shear rate curve) derivative of steady shear stress with respect to $\dot{\gamma}$, $(d\sigma_{xy}/d\dot{\gamma})$ versus $\dot{\gamma}$ for a family of β values. For stable shear flow the shear stress vs shear rate curve must be monotonic (positive slope everywhere). The maximum value of β that yields a monotonic curve of stress-shear rate is $\beta = 0.12$. The results from $\beta = 0.13$ showed *negative* values around shear rate of $0.01\,\mathrm{s}^{-1}$ (curve not shown).

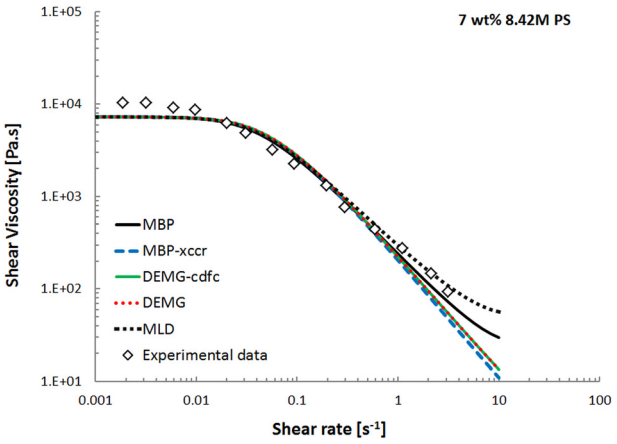

FIG. 11. The shear flow curve, η vs $\dot{\gamma}$, for a monodisperse PS solution 7% 8.42 M PS. Predictions are from various options of the family of models (see figure legend and Table I). Note that the results from the DEMG and DEMG-cdfc models effectively superpose since CDFC is diluted out of this semidilute system.

In Fig. 11 we compare the calculated shear flow curve for a 7 wt. % 8.42 M PS solution with experimental data [Pattamaprom and Larson (2001)]. We also compare the first normal stress difference with data in Fig. 12. In both cases, all the models approximately mimic the data. The MBP model improves the agreement with the experimental viscosity at high shear rates whereas the normal stress differences are under predicted. Note that the results from the DEMG and DEMG-cdfc models were very similar, which indicates the effect of CDFC is very weak for solutions as was the case in the extensional flows of semidilute solutions. The flow curve of MBP-xccr in Fig. 11 is very similar to those of DEMG models but the discrepancy from the experimental data is a little lower than that of DEMG models.

Figure 13 shows the simulation results of transient shear viscosity of a PS200K-S melt [Schweizer *et al*. (2004)]. All the models display similar trends to those found in steady shear flow of solutions with the DEMG-cdfc and MBP-xccr models performing best. The

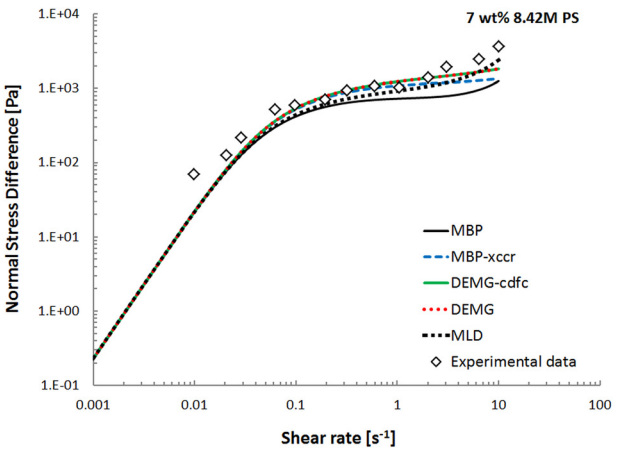

FIG. 12. The first normal stress difference for a monodisperse PS solution 7% 8.42 M PS is shown, N_1 vs $\dot{\gamma}$. Predictions are from various options of the family of models (see figure legend and Table I). Note that the results from the DEMG and DEMG-cdfc models are on top of each other since CDFC is diluted out of this system.

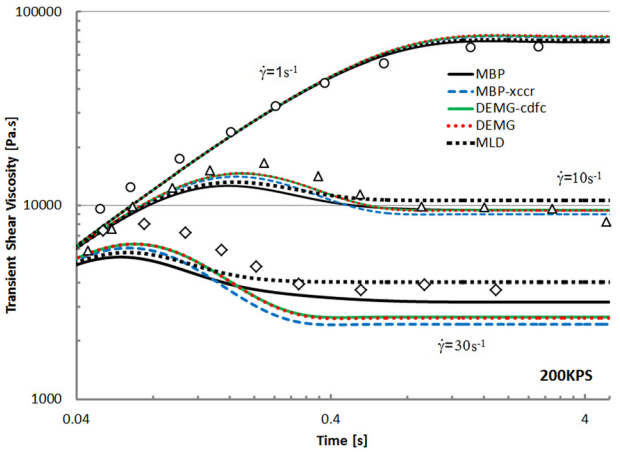

FIG. 13. Transient monodisperse 200 K-S PS melt at shear rates of 1, 10, and 30 s^{-1}. Since the net Kuhn bond orientation is low the effect of CDFC is negligible and the DEMG-cdfc model is approximately equal to the DEMG model. The poor agreement with data at 30 s^{-1} is due to the use of the differential form of the orientation evolution equation.

shear stress overshoot is missed by all models in fast shear flows, $\dot{\gamma} = 30\,s^{-1}$. This is caused by the differential form of the orientation evolution equation used in this work rather than the rigorous integral formulation [Larson (1984); Marrucci (1984)]. Using the original Doi–Edwards integral evolution equation, employing the universal orientation tensor will significantly improve these fast transient shear simulations at the expense of more complex simulation software.

VII. DISCUSSION/SUMMARY

We have constructed a mathematically and computationally simple toy molecular model that includes ED, CDFC, and CCR into the base DEMG toy model: The MBP model. This model is a natural next step in the systematic progression of increasingly detailed and complex molecular models for entangled linear flexible polymers. This point can be seen by noting that there are three essential components to the constitutive equation for a monodisperse polymer melt or an entangled semidilute solution. This can be seen by referencing the stress calculator Eq. (31). {Note that Eq. (31) or Eq. (35) can be generated directly from the stress-optical rule which is valid in both the linear and *nonlinear* flow regions [Larson (1988)].}

$$\boldsymbol{\sigma}(t) = 3 \underbrace{G_N(t)}_{\substack{\textit{Entanglement}\\ \textit{dynamics}}} \underbrace{\Lambda^2(t)}_{\substack{\textit{Stretch}\\ \textit{dynamics}}} \underbrace{\mathbf{S}_{tube}(t)}_{\substack{\textit{Orientation}\\ \textit{dynamics}}} . \tag{35}$$

The three fundamental components of any monodisperse constitutive relationship are; (1) A quantitative description of the orientation dynamics, Eq. (21), (2) a quantitative description of the stretch dynamics, Eq. (28), and (3) a quantitative description of the EDs, Eq. (27) [which are manifested in Eq. (35) through the nonlinear modulus $G_N(t)$ Eq. (32)]. The three essential constitutive equation components are, of course, all coupled and nonlinear. They also incorporate effects like CDFC in the time scales in their descriptions.

The original Doi–Edwards model assumed no stretch and no EDs only considering the orientation dynamics in Eq. (35) [Doi and Edwards (1986)]. Consequently, the original family of Doi–Edwards tube and reptation models is restricted to the linear viscoelastic region. To access more general, nonlinear flow situations, the Doi–Edwards model evolved naturally and systematically by next including the stretch dynamics to generate the DEMG model [Pearson *et al*. (1991); Mead *et al*. (1995); Mead and Leal (1995)]. The next step in the evolutionary progression was the MLD model which considered EDs in the form of CR in the restricted context of a *constant* net entanglement density [Mead *et al*. (1998)]. The new MBP model relaxes the final restriction of a constant entanglement density in order to access nonlinear flow phenomena far from equilibrium. In the above manner, we can see the logical and systematic progression/evolution of molecular models starting from the seminal work of de Gennes and Doi–Edwards.

The new MBP model generates extensional flow curves that are monotonic thinning (with a small kink near $\dot{\varepsilon}\tau_{s,eq} \approx 1$) for monodisperse PS melts qualitatively consistent with experiment. The results are sensitive to the specific functional form of CDFC used and the predictions could potentially be improved by modifying the expression for CDFC to fit the flow curve data [Eqs. (24)–(26)]. We have not performed this exercise but could do so in principle. We have used a shifted version of the specific functional form of CDFC calculated by Ianniruberto *et al*. (2012) which has a sound theoretical basis underlying it. For monodisperse PS solutions, the effects of CDFC are effectively diluted out and the classical tube model ladle shaped extensional flow curve is generated. The simulation results strongly suggest that CDFC is important in the prediction of rheological properties in nonlinear extensional flows of monodisperse PS melts. CCR is detrimental to the predictions in extensional flows but is important for the rheological properties in shear flows.

We have also provided a plausible explanation as to why the DEMG-cdfc model yields a monotonic thinning flow curve of monodisperse PS melts that are approximately equivalent to those predicted by the new MBP-xccr model, i.e., DEMG with ED on, CDFC on and CCR off. This may partially explain the previous apparent success of the mono and polydisperse MLD models in predicting phenomena such as the Cox–Merz rule even though the flow curves calculated assume a *constant* entanglement density [Mead (2011b)]. This suspicious coincidence masks the underlying details that are actually occurring in fast nonlinear flows of entangled polymers. Our new model simultaneously captures nonlinear flows and the entanglement microstructure modification that occurs in these fast flows.

Incorporating ED into the model allows the nonlinear phenomenon of shear modification to be captured by the model [Dealy and Wissbrun (1989)]. Shear modification manifests itself in linear polymer melts with high MW and broad molecular weight distribution (MWD) LCB. Direct measurement of the reduced modulus during or after shear or extension would provide an excellent test of the new ED model [Mead (2013)]. Note that current molecular constitutive models for polymer systems with LCB do not predict shear modification despite the fact that this is a prominent nonlinear property [McLeish and Larson (1998)].

Generalizing the new MBP model to polydisperse systems is straightforward and is performed in Appendix B. Having a generally applicable model for polydisperse systems that is easy to code and fast to execute has many practical applications in analytic rheology. We shall pursue applications such as MWD determination from transient extensional rheology experiments in future work.

Finally, knowledge of the melt entanglement density following polymer shaping operations (finite deformations) is crucially important with respect to determining the ultimate

mechanical properties of the part. Specifically, crystallization processes are severely impacted by the entanglement density of the melt [Yamazaki *et al*. (2006); Wang *et al*. (2009); Eder *et al*. (1990)]. The morphology of the resulting crystallites determines the physical and mechanical properties of the final product [Rastogi *et al*. (2003)]. Hence, the information gleaned from molecular models with ED, such as the MBP model, is directly relevant to polymer processing operations.

ACKNOWLEDGMENTS

The authors acknowledge Dr. Morton M. Denn's helpful comments and use of thecomputational facilities at the City College of New York. Partial financial support from the Materials Research Center and the Energy Research & Development Center of Missouri University of Science and Technology was also gratefully acknowledged.

APPENDIX A: DERIVATION

In this Appendix, we derive Eq. (5) in the main text, the relationship between the non-equilibrium tube disengagement time $\tau_d^1(N)$, the number of entanglements N, and the equilibrium terminal disengagement time, $\tau_{d,0}$. We start with the relationship between the tube length b and the Kuhn bond length a [Doi and Edwards (1986)]

$$Nb^2 = M_k a^2. \tag{A1}$$

Here, N is the number of entanglements (tube segments). The end-to-end distance of the tube segments and Kuhn bonds within them must be equal. M_k is the number of Kuhn segments of length a. Hence, the tube length b is related to the number of entanglements through

$$b = \frac{{M_k}^{1/2}}{N^{1/2}} a. \tag{A2}$$

The equilibrium tube contour length, $L_{eq} = Nb$, is a function of the number of entanglements N

$$L_{eq} = Nb = N^{1/2}\left({M_k}^{1/2} a\right). \tag{A3}$$

Note that L_{eq} is a monotonically increasing function of N.

The terminal tube disengagement time τ_d is related to the tube length through [Doi and Edwards (1986)]

$$\tau_d = \frac{{L_{eq}}^2}{\pi^2 D_c}. \tag{A4}$$

Here, $D_c = (kT/M\varsigma_o)$ is the curvilinear diffusion coefficient and ς_o is the monomeric friction coefficient. We define the equilibrium terminal disengagement time as $\tau_{d,0} = (L_{eq}^2/\pi^2 D_c) = (N_e M_k b^2/\pi^2 D_c)$, where N_e is the equilibrium number of entanglements. Substituting these expressions into Eq. (A4) above yields the result Eq. (5)

$$\tau_d^1(N) = \left(\frac{N}{N_e}\right)\tau_{d,0}. \tag{A5}$$

APPENDIX B: GENERALIZATION OF THE NEW EDS—CDFC MLD TOY MODEL TO POLYDISPERSE SYSTEMS

In this Appendix, we outline the manner in which the ideas presented in the main text can be generalized to describe polydisperse systems. In this section *i-j* subscripts denote components of the MWD and not tensor components [Mead (2007)].

The *ij* entanglement pair dynamics are described by the following equation which generalizes Eq. (1)

$$\dot{N}_{ij}(t) = \underbrace{\frac{N_{ij}^0 - N_{ij}(t)}{\tau_{d,i}^1(t)}}_{\substack{i\text{-chain tip diffusion}}} - \underbrace{\beta\left[(\boldsymbol{\kappa} : \mathbf{S}_{i,tube}) - \frac{\dot{\Lambda}_i(t)}{\Lambda_i} + \frac{\dot{\alpha}_i(t)}{\alpha_i}\right] N_{ij}(t)}_{\substack{\text{convective destruction of } ij \\ \text{entanglements}}} + \underbrace{\frac{N_{ij}^0 - N_{ij}(t)}{\tau_{d,j}^1(t)}}_{\substack{j \text{ matrix tip diffusion}}} . \tag{B1}$$

Here, $N_{ij}(t)$ represents the number of j entanglements on an i chain and $N_{ij}^0 = w_j N_{e,i} = w_j(M_i/M_e)$ represents the equilibrium number of j entanglements on an i-chain and $N_{e,i} = (M_i/M_e)$ is the total equilibrium number of net entanglements on an i chain. $N_{e,i}$ is a function of molecular weight and the molecular weight between entanglements which is assumed not to be affected by polydispersity.

The reptation time of an i-chain is modified by the number of current entanglements of all other chains on the i-chain [Eq. (5) and Appendix A)

$$\tau_{d,i}^1(t) = \left(\frac{N_i(t)}{N_{e,i}}\right)\tau_{d,i}(t) = \left(\frac{\sum_j N_{ij}(t)}{N_{e,i}}\right)\tau_{d,i}(t). \tag{B2}$$

Of course, CDFC as described in Sec. II A will also be present which will reduce $\tau_{d,i}(t)$ in fast flows.

The first approximation to try for the functional form of the reduced friction CDFC is that used in our first paper [Park *et al.* (2012)]

$$\frac{\varsigma(t)}{\varsigma_{eq}} = \frac{\tau_{s,i}(t)}{\tau_{s,i}^0} = \frac{\tau_{d,i}(t)}{\tau_{d,i}^0} = 1 - k\ \underbrace{\mathbf{S}_{Kuhn,i}}_{\substack{\text{test chain} \\ \text{Kuhn bond} \\ \text{orientation}}} : \underbrace{\sum_j w_j \mathbf{S}_{Kuhn,j}}_{\substack{\text{net matrix Kuhn} \\ \text{bond orientation}}} . \tag{B3}$$

The above expression is written for a polydisperse system where the components are denoted by subscripts and w_j represents the weight fraction of MW component j. The effect of Kuhn bond concentration is accounted for in the weight fraction of matrix polymers and/or solvent. The relative orientation of the test chain and the matrix is quantified by the double dot product of the two orientations.

This is one possible algorithm that we propose for CDFC of the polydisperse MLD model. Other functional forms for the dependence of the friction factor on relative test chain—matrix Kuhn bond alignment can be tried too. For example, by generalizing Eq. (24), we see that

$$\begin{aligned}\frac{\varsigma(t)}{\varsigma_{eq}} = \frac{\tau_{s,i}(t)}{\tau_{s,i}^0} = \frac{\tau_{d,i}}{\tau_{d,i}^0} = f\left(\mathbf{S}_{Kuhn,i} : \sum_j w_j \mathbf{S}_{Kuhn,j}\right) = 0.02239\left[\mathbf{S}_{Kuhn,i} : \sum_j w_j \mathbf{S}_{Kuhn,j}\right]^{-1.65} \\ = 0.02239\left[x_i^2 \mathbf{S}_{tube,i} : \sum_j w_j x_j^2 \mathbf{S}_{tube,j}\right]^{-1.65} .\end{aligned} \tag{B4}$$

This function approximates the monodisperse case, Eq. (24). Note that for most common commercial molecular weight distributions, the effects of CDFC will largely disappear due to the lower overall level of Kuhn bond orientation in polydisperse systems under ordinary flow conditions. The low MW components effectively act as solvent for the high MW components [Mead (2011b)].

The i-component partially disentangled chain stretch equation remains unchanged

$$\dot{\Lambda}_i(t) = \underbrace{-\left[\frac{\dot{\alpha}_i(t)}{\alpha_i(t)}\right]\Lambda_i(t)}_{\substack{\text{stretch reduction}\\ \text{due to disentanglement}}} + \underbrace{(\boldsymbol{\kappa} : \mathbf{S}_i)\Lambda_i}_{\text{affine stretch}} - \underbrace{k_{s,i}(t)\left(\frac{\Lambda_i - 1}{\tau_{s,i}(t)}\right)}_{\text{chain retraction}} + \underbrace{\frac{1}{2}\left(1 - |\mathbf{S}_{tube,i}|\right)(\Lambda_i - 1)\dot{\Phi}}_{\text{CCR tube shortening}}, \tag{B5}$$

where $\dot{\Phi}$ is the fractional rate of matrix entanglement renewal, $\dot{\Phi} \equiv \sum_j w_j\{(\boldsymbol{\kappa} : \mathbf{S}_{tube,j}) - [\dot{\Lambda}_j(t)/\Lambda_j] + [\dot{\alpha}_j(t)/\alpha_j] + (1/\Lambda_j^2\tau_{d,j})\}$, and $|\mathbf{S}_{tube,i}|$ is the magnitude of the i-chain tube orientation, $|\mathbf{S}_{tube,i}| = \sum_j w_j|\mathbf{S}_{tube,ij}|$. The nonlinear spring factor $k_{s,i}(t)$ is defined by Eq. (30) for each i chain.

The maximum stretch ratio factor $\alpha_i(t) \equiv [\Lambda_{i,\max}(t)/\lambda_{\max}]$ needs to be calculated to solve the stretch equation. The easiest way to accomplish this is using the definition of $\alpha_i(t)$ along with the known entanglement pair dynamics, $N_{ij}(t)$

$$\alpha_i(t) \equiv \frac{\Lambda_{i,\max}(t)}{\lambda_{\max}} = \left[\frac{N_{e,i}}{\sum_j N_{ij}(t)}\right]^{1/2}. \tag{B6}$$

The factor $\dot{\alpha}_i(t)$ in Eq. (B6) can be calculated numerically at each time step rather than solving the ordinary differential equation for $\alpha_i(t)$.

Similarly, the orientation of the ij entanglement pairs obeys the following differential equation [Mead (2007)]:

$$\hat{S}_{tube,ij}(t) + 2\big(\boldsymbol{\kappa}(t) : \mathbf{S}_{tube,ij}(t)\big)\mathbf{S}_{tube,ij} + \left(\frac{1 - S_{Kuhn}}{\tau_{d,ij}(t)}\right)\left(\mathbf{S}_{tube,ij} - \frac{1}{3}\underline{\underline{\boldsymbol{\delta}}}\right) = 0, \tag{B7}$$

where the ij entanglement disengagement time $\tau_{d,ij}$ is

$$\frac{1}{\tau_{d,ij}(t)} = \frac{1}{\Lambda_i^2(t)\tau_{d,i}(t)} + \left(\frac{1}{\Lambda_i}\right)\left[(\boldsymbol{\kappa} : \mathbf{S}_{tube,j}) - \frac{\dot{\Lambda}_j(t)}{\Lambda_j} + \frac{\dot{\alpha}_j(t)}{\alpha_j} + \frac{1}{\Lambda_j^2(t)\tau_{d,j}(t)}\right]. \tag{B8}$$

And S_{Kuhn} is the net matrix Kuhn bond orientation, $S_{Kuhn} = \sum_i w_i S_{Kuhn,i} \approx \sum_i w_i x_i^2 |\mathbf{S}_{tube,i}|$.

Of course, the Kuhn bond conformation dependence (CDFC) of the disengagement and stretch times is applicable. This is why we write both $\tau_{d,i}(t)$ and $\tau_{s,i}(t)$ as functions of time.

Additionally, the effect of "solventlike" entanglements with respect to stretch processes needs to be accounted for in polydisperse systems. This can be accomplished in the manner described in Mishler and Mead (2013a, 2013b), where entanglements with an average lifetime less than the Rouse time act as solvent with respect to stretch relaxation processes.

The expression for the stress is more involved and requires some discussion. Consider the expression for the stress from the polydisperse MLD model without EDs

$$\boldsymbol{\sigma}(t) = 3\sum_i (w_i G_N^0)\, k_{s,i}\Lambda_i^2 \mathbf{S}_{tube,i} = 3\sum_i \underbrace{(w_i G_N^0)}_{\substack{i\ chain\\ modulus}} k_{s,i}\Lambda_i^2 \underbrace{\sum_j w_j \mathbf{S}_{tube,ij}(t)}_{\mathbf{S}_{tube,i}} . \tag{B9}$$

Here, $G_N^0 \equiv (\rho RT/M_e)$ represents the equilibrium value of the modulus and M_e is the molecular weight between entanglements which for the MLD model is a constant. The factor $k_{s,i}$ represents the effects of the i-component finitely extensible nonlinear spring, Eq. (30). In Eq. (B9), we have assumed that $G_N = \sum_i G_{N,i} = \sum_i (\rho_i RT/M_e)$. However $\rho_i = w_i\rho$ so that $G_{N,i} = w_i(\rho RT/M_e) = w_i G_N^0$, hence Eq. (B9).

We need to generalize this expression to allow for varying degrees of deformation induced disentanglement, where the molecular weight between entanglements varies from component to component in the MWD. The nonequilibrium modulus can be written as $G_{N,i} \equiv [\rho_i RT/M_{e,i}(t)]$. Here, $M_{e,i}(t)$ is the molecular weight between entanglements on the i-component. In the polydisperse case with varying degrees of disentanglement two things in the expression for G_N change: $\rho_i = w_i\rho$ the number of i-strands per unit volume and the molecular weight between entanglements on i-component chains $M_e(t) \equiv [M_i/N_i(t)]$.

With these two changes in mind, we can write the nonequilibrium i-chain modulus $G_{N,i}$ by analogy to the monodisperse equilibrium case

$$\frac{\rho_i RT}{M_{e,i}(t)} = w_i\left(\frac{N_i(t)}{N_{e,i}}\right)G_N^0 = \underbrace{w_i G_N^0\left(\frac{\sum_k N_{ik}(t)}{N_{e,i}}\right)}_{\substack{i\ chain\\ modulus}} . \tag{B10}$$

So, using the above expression for the i-chain modulus, we can write the stress for a system with arbitrary polydispersity as

$$\boldsymbol{\sigma}(t) = 3\sum_i \underbrace{\left(w_i\left(\frac{\sum_k N_{ik}(t)}{N_{e,i}}\right)G_N^0\right)}_{i\ chain\ modulus} k_{s,i}(t)\Lambda_i^2(t) \underbrace{\sum_j w_j \mathbf{S}_{tube,ij}(t)}_{\mathbf{S}_{tube,i}} . \tag{B11}$$

As with the monodisperse case, polydisperse systems are predicted to display shear modification since $N_{ik}(t)$ will recover its equilibrium entanglement density $N_{e,i}$ on reptation time scales which can be extremely long for high molecular weight entanglement pairs.

We anticipate that for typical commercial polydisperse polymer melts most of the effects of CDFC discussed in this paper will disappear since the average level of Kuhn bond orientation will be low. However, this will not be the case for the EDs effects. The effects of ED such as shear modification will manifest themselves for broad polydisperse melts with high molecular weight tails [Dealy and Tsang (1981); Rokudai (1979)].

APPENDIX C: INTERNAL DETAILS OF THE MODEL CALCULATIONS

In this Appendix, we detail the inner model workings underlying Fig. 3. In this way, the mechanisms responsible for the observed uniaxial flow curves can be readily understood. In Fig. 14 the steady state orientation as a function of extension rate is displayed for the system described in Fig. 3. Similarly, Fig. 15 displays the steady state Kuhn bond

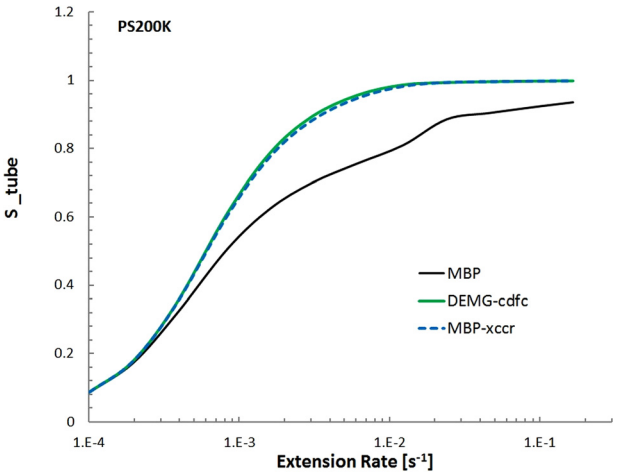

FIG. 14. Steady state orientation as a function of extension rate for monodisperse PS200K at 130 °C [Bach *et al.* (2003)]. Predictions are from various options of the family of models (see figure legend and Table I). This allows us to determine the orientation levels when stretch and CDFC commence. The equilibrium stretch relaxation time is $\tau_{s,eq} \approx 94$ s which does not include the effects of CDFC.

orientation as a function of extension rate. An inflection point is seen in the curves at $\dot{\varepsilon}\tau_{s,eq} \approx 1$ corresponding to the onset of significant stretch. CDFC effects set in for Kuhn bond orientations greater than 0.1. Finally, Fig. 16 displays CDFC, $(\varsigma/\varsigma_{eq}) = (\tau_{s,i}/\tau^0_{s,i})$, as a function of extension rate and the onset of CDFC effects is clearly shown. All of the above figures can be correlated to the extensional viscosity flow curve shown in Fig. 3 and obvious conclusions concerning the causes for the various features can be drawn. In particular, precisely when CDFC is activated relative to $\dot{\varepsilon} \approx (1/\tau_{s,eq})$ is impacted by whether ED and CCR are on or off. Choosing a different functional form for CDFC can in principle modify precisely when CDFC is activated relative to $\dot{\varepsilon} \approx (1/\tau_{s,eq})$.

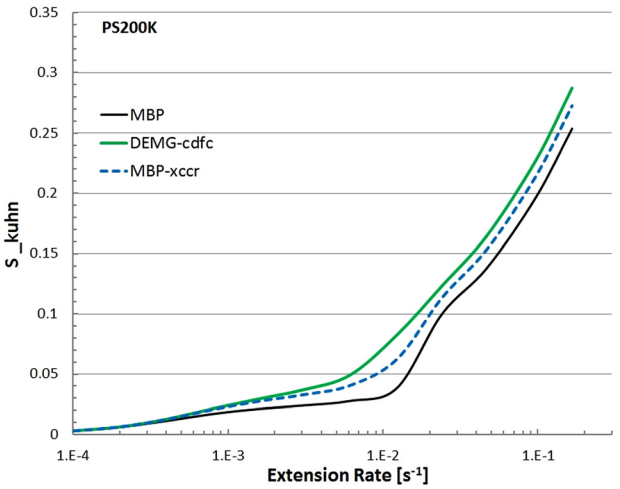

FIG. 15. Steady state Kuhn bond orientation as a function of extension rate for monodisperse PS200K at 130 °C. Predictions are from various options of the family of models (see figure legend and Table I). The equilibrium stretch relaxation time is $\tau_{s,eq} \approx 94$ which doesn't include the effects of CDFC. CDFC commences when Kuhn bond orientation is greater than 0.10.

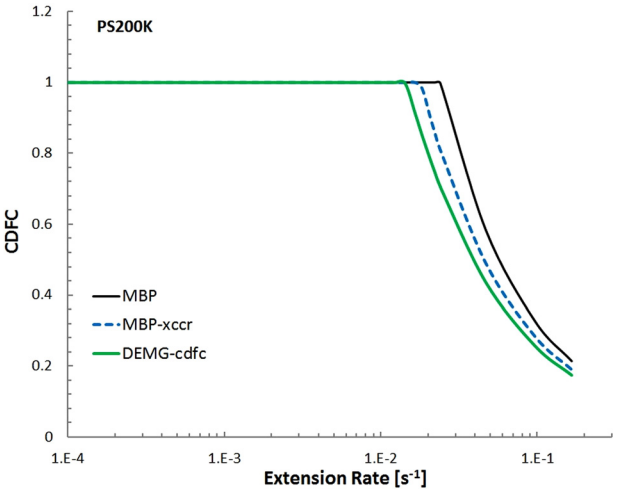

FIG. 16. Steady state ratio of $(\varsigma/\varsigma_{eq}) = (\tau_{s,i}/\tau^0_{s,i})$ as a function of extension rate for monodisperse PS200K at 130 °C. The equilibrium stretch relaxation time is $\tau_{s,eq} \approx 94$ s which does not include the effects of CDFC. Predictions are from various options of the family of models (see figure legend and Table I).

References

Acharya, M. V., P. K. Bhattacharjee, D. A. Nguyen, and T. Sridhar, "Are entangled polymeric solutions different from melts?," AIP Conf. Proc. **1027**, 391–393 (2008).

Andreev, M., R. N. Khaliullin, R. J. A. Steenbakkers, and J. D. Schieber, "Approximations of the discrete slip-link model and their effect on nonlinear rheology predictions," J. Rheol. **57**, 535–557 (2013).

Bach, A., K. Almal, O. Hassager, and H. K. Rasmussen, "Elongational viscosity of narrow molar mass distribution polystyrene," Macromolecules **36**, 5174–5179 (2003).

Baig, C., V. G. Mavrantzas, and M. Kroger, "Flow effects on melt structure and entanglement network of linear polymers: Results from a non-equilibrium molecular dynamics study of a polyethylene melt in steady shear," Macromolecules **43**, 6886–6906 (2010).

Bhattacharjee, P. K., J. P. Oberhauser, G. H. McKinley, L. G. Leal, and T. Sridhar, "Extensional rheometry of entangled solutions," Macromolecules **35**, 10131–10148 (2002).

Cohen, A., "A Padé approximant to the inverse Langevin function," Rheol. Acta **30**, 270–273 (1991).

Dealy, J. M., and K. F. Wissbrun, *Melt Rheology and Its Role in Plastics Processing* (Van Norstrand Reinhold, New York, 1989).

Dealy, J. M., and Wm. K.-W. Tsang, "Structural time dependency in the rheological behavior of molten polymers," J. Appl. Poly. Sci. **26**, 1149–1158 (1981).

Desai, P. S., and R. G. Larson, "Constitutive model that shows extension thickening for entangled solutions and extension thinning for melts," J. Rheol. **58**, 255–279 (2014).

Doi, M., and S. F. Edwards, *The Theory of Polymer Dynamics* (Oxford Science, Oxford, 1986).

Doi, M., D. S. Pearson, J. Kornfield, and G. G. Fuller, "Effect of nematic interaction in the orientational relaxation of polymer melts," Macromolecules **22**, 1488–1490 (1989).

Eder, G., H. Janeschitz-Kriegl, and S. Liedauer, "Crystallization processes in quiescent and moving polymer melts under heat transfer conditions," Prog. Poly. Sci. **15**, 629–714 (1990).

Everaers, R., S. K. Sukumaran, G. S. Grest, C. Svaneburg, A. Sivasubramanian, and K. Kremers, "Rheology and microscopic topology of entangled polymeric liquids," Science **303**, 823–827 (2004).

Flory, P. J., *Statistical Mechanics of Chain Molecules* (Interscience, New York, 1969).

Graham, R. S., A. E. Likhtman, T. C. B. McLeish, and S. T. Milner, "Microscopic theory of linear, entangled polymer chains under rapid deformation including chain stretch and convective constraint release," J. Rheol. **47**, 1171–1200 (2003).

Huang, Q., O. Mednova, H. K. Rasmussen, N. J. Alvarez, A. L. Skov, K. Almdal, and O. Hassager, "Concentrated polymer solutions are different from melts: Role of entanglement molecular weight," Macromolecules **46**, 5026–5035 (2013).

Ianniruberto, G., A. Brasiello, and G. Marrucci, "Friction coefficient does not stay constant in nonlinear viscoelasticity," in *Proceedings of the 7th Annual European Rheology Conference* (Università degli Studi di Napoli Federico II, Naples, 2011), p. 61.

Ianniruberto, G., A. Brasiello, and G. Marrucci, "Simulation of fast shear flows of PS oligomers confirm monomeric friction reduction in fast elongational flows of monodisperse PS melts as indicated by rheooptical data," Macromolecules **45**, 8058–8066 (2012).

Ianniruberto, G., and G. Marrucci, "On compatibility of the Cox-Merz rule with the model of Doi and Edwards," J. Non-Newtonian Fluid Mech. **65**, 241–246 (1996).

Ianniruberto, G., and G. Marrucci, "A simple constitutive equation for entangled polymers with chain stretch," J. Rheol. **45**, 1305–1318 (2001).

Ianniruberto, G., and G. Marrucci, "Convective constraint release revisited," J. Rheol. **58**, 89–102 (2014).

Larson, R. G., "A constitutive equation for polymer melts based on partially extending strand convection," J. Rheol. **28**, 545–572(1984).

Larson, R. G., *Constitutive Equations for Polymer Melts and Solutions* (Butterworths, Boston, 1988).

Leblans, P. J. R., and C. Bastiaansen, "Shear modification of low density polyethylene: Its origin and its effect on the basic rheological functions of the melt," Macromolecules **22**, 3312–3317 (1989).

Likhtman, A. E., and T. C. B. McLeish, "Quantitative theory for linear dynamics of linear entangled polymers," Macromolecules **35**, 6332–6343 (2002).

Marrucci, G. G., in *Advances in Transport Processes*, edited by A. S. Majumdar and R. A. Mashelkar (John Wiley & Sons, New York, 1984), Vol. V.

McLeish, T. C. B., and R. C. Ball, "A molecular approach to the spurt effect in polymer melt flow," J. Poly. Sci. Part B: Poly. Phys. **24**, 1753–1745 (1986).

McLeish, T. C. B., and R. G. Larson, "Molecular constitutive equations for a class of branched polymer: the pom-pom polymer," J. Rheol. **42**, 81–110 (1998).

Mead, D. W., "Development of the 'binary interaction' theory for entangled polydisperse linear polymers," Rheol. Acta **46**, 369–395 (2007).

Mead, D. W., "Derivation of the 'switch function' in the Mead-Larson-Doi theory," Rheol. Acta **50**, 631–643 (2011a).

Mead, D. W., "Analytic derivation of the Cox-Merz rule using the MLD 'toy' model for polydisperse linear polymers," Rheol. Acta **50**, 837–866 (2011b).

Mead, D. W., "Small amplitude oscillatory shear flow superposed on parallel or perpendicular steady shear of polydisperse linear polymers: The MLD model," J. Non-Newtonian Fluid Mech. **195**, 99–113 (2013).

Mead, D. W., D. Yavich, and L. Leal, "The reptation model with chain stretching I: Basic equations and general properties," Rheol. Acta **34**, 339–360 (1995).

Mead, D. W., and L. Leal, "The reptation model with chain stretching II: Steady flow properties," Rheol. Acta **34**, 360–383(1995).

Mead, D. W., R. G. Larson, and M. Doi, "A molecular theory for fast flows of entangled polymers," Macromolecules **31**, 7895–7914 (1998).

Mewis, J., and M. M. Denn, "Constitutive equations based on the transient network concept," J. Non-Newtonian Fluid Mech. **12**, 69–83 (1983).

Mishler, S. D., and D. W. Mead, "Application of the MLD 'toy' model to extensional flows of broadly polydisperse linear polymers: Model development," J. Non-Newtonian Fluid Mech. **197**, 61–79 (2013a).

Mishler, S. D., and D. W. Mead, "Application of the MLD 'toy' model to extensional flows of broadly polydisperse linear polymers: Comparison to experimental data sets," J. Non-Newtonian Fluid Mech. **197**, 80–90 (2013b).

Park, J., D. W. Mead, and M. M. Denn, "Stochastic simulation of entangled polymeric liquids in fast flows: Microstructure modification," J. Rheol. **56**, 1057–1082 (2012).

Pattamaprom, C., and R. G. Larson, "Constraint release effects in monodisperse and bidisperse polystyrenes in fast transient shearing flows," Macromolecules **34**, 5229–5237 (2001).

Pearson, D. S., E. A. Herbolzhiemer, N. Grizzuti, and G. Marrucci, "Transient behavior of entangled polymers at high shear rates," J. Polymer Sci., Part B: Poly. Phys. Ed. **29**, 1589–1597 (1991).

Rastogi, R., L. Kurelec, J. Cuijpers, D. Lippits, M. Wimmer, and P. J. Lemstra, "Disentangled state in polymer melts: A route to ultimate physical and mechanical properties," Macromol. Mater. Eng. **288**, 964–970 (2003).

Rokudai, M., "Influence of shearing history on the rheological properties and processability of branched polymers," J. Appl. Poly. Sci. **23**, 463–471 (1979).

Schweizer, T., J. van Meerveld, and H. C. Ottinger, "Nonlinear shear rheology of polystyrene melt with narrow molecular weight distribution—Experiment and theory," J. Rheol. **48**, 1345–1363 (2004).

Treloar, L. R. G., *The Physics of Rubber Elasticity*, 3rd ed. (Oxford University, Oxford, 1975).

Tzoumanekas, C., and Theodorou, D. N., "Topological analysis of linear polymer melts: A statistical approach," Macromolecules **39**, 4592–4604 (2006).

Wang, X., R. Liu, M. Wu, Z. Wang, and Y. Huang, "Effect of chain disentanglement on melt crystallization behavior of isotactic polypropylene," Polymer **50**, 5824–5827(2009).

Yamaguchi, M., and M. H. Wagner, "Impact of processing history on rheological properties for branched polypropylene," Polymer **47**, 3629–3635 (2006).

Yamazaki, S., F. Gu, K. Watanabe, K. Okada, A. Toda, and M. Hikosaka, "Two-step formation of entanglement from disentangled polymer melt detected by using nucleation rate," Polymer **47** 6422–6428 (2006).

Yaoita, T., T. Isaki, Y. Masubuchi, H. Watanabe, G. Ianniruberto, and G. Marrucci, "Primitive chain network simulation of elongational flows of entangled linear chains: Stretch/orientation induced reduction of monomeric friction," Macromolecules **45**, 2773–2782 (2012).

Yaoita, T., Y. Masubuchi, and H. Watanabe, "Concept of stretch/orientation reduction tested with a simple constitutive equation," Nihon Reoroji Gakkaishi **42**, 207–213 (2014).